



Holocene vertical velocity fields in the Calabrian Arc (southern Italy): New insights from uplifted sea-level markers in the Crotona Peninsula

Marco Liberatore^{*}, Elsa Gliozzi, Paola Cipollari, Domenico Cosentino

Dipartimento di Scienze, Università Degli Studi Roma Tre, Italy

ARTICLE INFO

Handling Editor: Dr Giovanni Zanchetta

ABSTRACT

The study of fossil coastlines is one of the most widely used methods to unravel the vertical movements of the Earth's solid surface. All along the coast of the Calabrian Subduction Arc, well preserved Pleistocene marine terrace sequences document a protracted uplift history. Although Pleistocene vertical movements have been extensively explored, the Holocene history is not well understood. Numerous uplifted coastlines of the Holocene period have been studied along the Tyrrhenian side of Calabria, but the Ionian coastal sector is considerably under-studied. Our new data from the coast of the Crotona Peninsula fill this crucial data-gap. AMS ¹⁴C dating of seventeen sea level markers, elevated above the current mean sea level, show ages between 2300 and 7000 Cal. Yr BP. The elevation of the markers was corrected for the paleo sea level using the most updated GIA models ICE-6G (VM5a) and ICE-7G (VM7). We found that a coastline dated to 7 ka shows uplift rates of 0.8 mm/yr, consistent with late Pleistocene uplift rates (≈ 0.8 mm/yr). In contrast, a 2.3 ka coastline was uplifted by only 1 m, resulting in lower uplift rates of ≈ 0.5 mm/yr. However, there are clues that the abandonment of this younger coastline may have occurred with a rapid uplift pulse. Reconstructing the past vertical movements of the Crotona Peninsula reveals an unsteady uplift history. At some times fast uplift rates are required, while for other periods, lasting as long as 3–4 kyr, the uplift rate is slower or zero. An uplift history consisting of periods of accelerated uplift, or even coseismic pulses, would also explain the difference in uplift rates between short term (<5 ka) and long term (>5 ka) markers through a metric we have defined as *uplift rate sensitivity*. Understanding the details of this uplift history has social relevance. The co-seismic uplift hypothesis requires further investigation but if confirmed would likely affect the seismic and tsunami hazard of the Crotona Peninsula. Similarly, the unsteady uplift rate would cause a risk given the current rapid rate of global sea level rise. Periods of sustained vertical stability would increase the risk of flooding even in areas characterized by long-term uplift and thus considered safe.

1. Introduction

The Calabrian Arc defines the upper plate of the Ionian Subduction System. In this geodynamic setting, the Ionian oceanic lithosphere is underthrust beneath the Calabrian continental block and the Tyrrhenian microplate (e.g., Faccenna et al., 2003) (Fig. 1). Evidence of such dynamics is a Wadati-Benioff plane dipping down to 400 km and an active volcanic arc in correspondence with the 150 km isobath of the subducting slab. From a tectonic point of view, the arc is now experiencing uplift as illustrated by instrumental records (Braitenberg et al., 2011; Serpelloni et al., 2013; Spampinato et al., 2013). Uplift is thought to have started since Serravallian-lower Tortonian (13.8–11 Ma) times, as witnessed by the age of the highest marine deposits in the Sila Massif

(Magri et al., 1963; Ogniben, 1973; ISPRA, CARG 561-San Giovanni in Fiore) and continued through the Pleistocene, producing the well-known flights of marine terraces along much of the coast (Miyauchi, 1994; Dumas et al., 1995; Dumas and Raffy, 1996; Cucci, 2004; Bianca et al., 2011; Monaco et al., 2017; Cerrone et al., 2021b). Fossil sea floors from the earliest Pleistocene can now be found up to 1300 m elevation (Miyauchi, 1994), but to constrain uplift on a shorter period, the elevation of the MIS 5.5 marine terrace, representing the Last Interglacial Maximum (≈ 125 ka), is often considered (e.g., Bordoni and Valensise, 1999; Tam and Yokoyama, 2021). Deposits of this age, related to a sea-level ≈ 8 m higher than the current one (Ferranti et al., 2006), can now be located at elevations of up to tens of meters (Cerrone et al., 2021b and references therein) (Fig. 1). The highest elevation for a

^{*} Corresponding author.

E-mail address: marco.liberatore@uniroma3.it (M. Liberatore).

MIS5.5 marine terrace occurs in the Strait of Messina, where the inner edge of the MIS 5.5 terrace reaches an elevation up to 175 m. At Capo Vaticano, the position of the MIS 5.5 marine terrace is debated. According to Dai Pra et al. (1992), Miyauchi (1994), and Anzidei et al. (2013), it is around 90–120 m in the SW sector and 48–60 m near Briatico and Vibo Marina. In contrast, Barrier (1990), Tortorici et al. (2003), Bianca et al. (2011) believe that the elevation of the MIS 5.5 marine terrace varies even between 216 and 285 m. In other areas of Calabria, the MIS 5.5 marine terrace elevation is lower: in the Tyrrhenian coastal area near Gioia Tauro, it is about 65 m (Cosentino and Gliozi, 1988) while it is only 9–12 m at Diamante (Carobene et al., 1986). On the Ionian coast between Locri and Catanzaro, it has been tentatively placed at 92 m through stratigraphic correlation with a section at Reggio Calabria (Dumas et al., 1995; Dumas and Raffy, 1996). This value would agree with the 100 m terrace stratigraphically dated to MIS 5.5 at San Leonardo di Cutro on the Crotone Peninsula (Cosentino and Gliozi, 1988; Gliozi, 1988). Similarly, in the Gulf of Sibari, deposits related to the last interglacial have been dated by aminostratigraphy at an elevation of 114 m (Cucci, 2004). Vertical uplift rates close to or greater than 1 mm/yr are thus generally achieved throughout much of the Calabria region. However, Upper Pleistocene stratigraphic markers do not provide accurate information on the current state of the vertical velocity field of an area. For this purpose, Holocene sea-level markers, in such active tectonic frames, are commonly searched. They can reveal high-frequency fluctuations in the long-term trend but also, they represent a powerful way to understand mechanisms and dynamics of vertical movements of the Earth's surface. Unfortunately, Holocene sea-level markers in Calabria are limited to a few sites. This is mainly

due to the physiography of the Calabrian Peninsula. Generally, the presence of a sandy coast prevents the preservation of ancient coastlines through time. Only on the Tyrrhenian side, between the Messina Strait and Capo Vaticano, where rocky coasts are more common, have a significant number of Holocene sea-level markers been preserved and investigated.

Antonoli et al. (2006) reported Holocene uplift rates between 1.6 and 2.7 mm/yr and between 1.2 and 1.6 mm/yr in two Tyrrhenian-side Calabrian localities (4 & 7 in Fig. 1). Ferranti et al. (2007) reported new evidence of raised Holocene coastlines from the Calabrian Messina Strait (5 & 6 & 8 in Fig. 1). From those sites, sea-level markers between ≈ 2 and ≈ 5 ka were related to coastlines currently between 1 and 3 m in elevation. The authors interpreted their position as the dual result of recurring coseismic displacements and periods of steady uplift. In all these sites, the curve of sea-level rise predicted by the glacio-isostatic adjustment (GIA) model of Lambeck et al. (2004) was used to account for paleo sea level. In addition, evidence of raised Holocene coastlines from Capo Vaticano (2 & 3, Fig. 1) were described by Spampinato et al. (2014), by considering bio-geomorphological sea level markers. They identified four discrete levels between ≈ 0.7 and ≈ 2.3 m above mean sea level (a.m.s.l.) dated between ≈ 2 and ≈ 6 ka. The abrupt change between each level was considered to have occurred coseismically. In contrast, for the northern side of Capo Vaticano (Site 1 in Fig. 1), Anzidei et al. (2013) supposed steady uplift in the last 1800 yr BP. Based on archaeological remains of structures with a clear relationship with the sea level, namely a fish tank and a breakwater, they proposed a continuous uplift rate of 0.65 mm/yr. Both the papers refer to the Lambeck et al. (2011) curve for paleo sea-level correction. On the Ionian side of

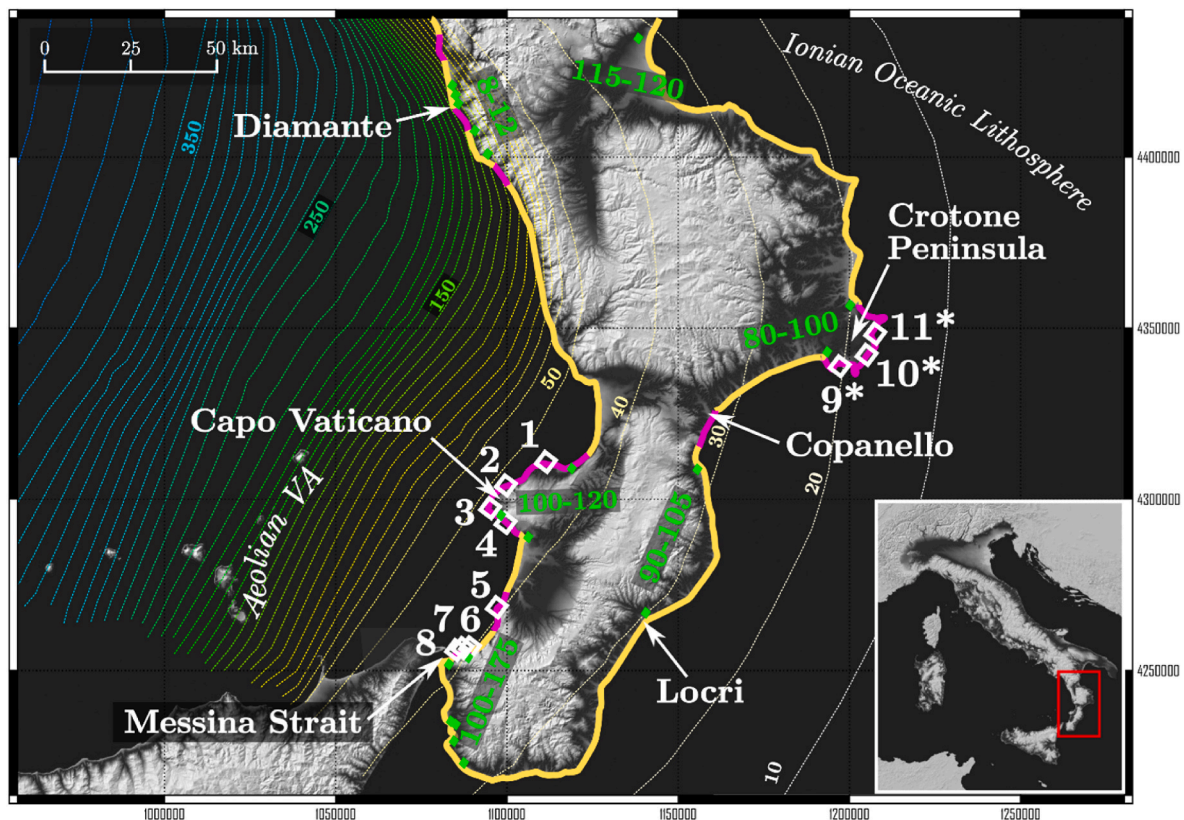


Fig. 1. The Calabrian Arc and the Ionian Subduction System. Isobaths (km) of the subducting slab are the coloured SW-NE striking lines (<https://edsf13.ingv.it/index.html>). The Aeolian VA (Aeolian Volcanic Arc) is the active volcanic arc of the subducting system. Coasts are coloured depending on the physical geography: yellow for mainly sandy coasts, pink for mainly rocky coasts. Elevation of the MIS 5.5 marine terrace is reported with green numbers, position of the observation is the small green square. White empty squares are the sites of the Holocene sea-level markers; * are the investigated localities in this study. 1- Briatico (BRI) (Anzidei et al., 2013); 2–3 – Capo Vaticano (CPV1-5) (Spampinato et al., 2014); 4 – Ioppolo (IOP) (Antonoli et al., 2006); 5 – Palmi (PAL) (Ferranti et al., 2007); 6,7,8 – Punta Paci (PPC), Scilla (SCI), Marina di San Gregorio (MSG) (Antonoli et al., 2006; Ferranti et al., 2007); 9,10,11 – Spiaggia dei Gigli (GIG), Spiagge Rosse (SPR) (Pirazzoli et al., 1997), Spiaggia di Curmo (CUR).

Calabria, the only evidence of Holocene uplift is reported by Pirazzoli et al. (1997), by considering bio-geomorphological sea-level markers. Along the beach of Soverato (near Copanello in Fig. 1), these authors found a beachrock reaching a maximum elevation of 1–1.5 m. In the Crotona Peninsula, around Le Castella village (Site 9 × in Fig. 1), the authors reported an abrasion platform at 1 m a.m.s.l. However, datable material was lacking in both these localities. The only radiocarbon dated sample is from the bay of “Spiagge Rosse” (Site 10 × in Fig. 1), where an emerged beachrock can be observed up to 1.0 ± 0.2 m a.m.s.l. A sample of calcareous algae yielded an age of 2990 ± 60 yr BP (not calibrated), providing the means to calculate the only Holocene uplift rate value along the entire Ionian coast of Calabria. In this context, it is clear that the Holocene uplift history of the Ionian coast of Calabria is poorly understood, even if the region has been suggested to be a potentially suitable place to search for Holocene evidence of uplift (Cosentino and Gliozzi, 1988; Gliozzi, 1988; Pirazzoli et al., 1997).

In this study, the Ionian coasts of Calabria between the village of Copanello, to the south, and the promontory of Capo Colonna, to the north, were explored for Holocene sea level markers (Fig. 1). Field observations confirmed numerous traces of past sea level, at elevations well above the current mean sea level (MSL), several of which contained appropriate material for dating. Following corrections for paleo sea level, we consider this new suite of Holocene uplift constraints, together with constraints from other locations in Calabria and longer-term uplift rates, to evaluate previously posed hypotheses on the uplift mechanisms.

2. Study area

2.1. Geological setting

The Crotona Peninsula is the easternmost point of the Calabria region. Outcropping units belong to the onshore portion of the Crotona Basin. It extends offshore for several kilometres and it is interpreted to be a forearc basin, developed between the Ionian accretionary complex and the Calabrian terrain (Zecchin et al., 2012; Massari and Prosser, 2013; Zecchin et al., 2018). Sediment deposition within the basin started since the Serravallian (13.82–11.63 Ma) (Massari and Prosser, 2013) and continues currently offshore. Two main lithologies outcrop in the Crotona Peninsula: a marly-clay unit known as the “argilla marnosa di Cutro” (marly clay of Cutro) and the younger Pleistocene calcarenites, including the Sant’Anna Lake (Chibanian), Soverito (Tyrrhenian), and Capo Cimiti (upper Pleistocene) synthems (ISPRA CARG project 577-Isola di Capo Rizzuto and 571-Crotona). The “argilla marnosa di Cutro” is a marine unit representing a deep-sea environment, dated to the Upper Pliocene (Piacenzian) - Lower Pleistocene (middle Calabrian) (Zecchin et al., 2012). It widely crops out in the study area, representing the substrate of the Middle Pleistocene and Upper Pleistocene synthems. These latter deposits overlie the “argilla marnosa di Cutro” through a sharp angular unconformity. Furthermore, because the Middle-Upper Pleistocene deposits are much less erodible than the underlying clay, they form a classic caprock-like morphology. When this caprock is dismembered as result of erosion, the “argilla marnosa di Cutro” crops out, typically hosting large fields of badlands. The Middle-Upper Pleistocene deposits, mainly consisting of calcarenites, form the prominent step-like profile of marine terraces recognizable along the entire Crotona Peninsula. The main lithology of the Middle-Upper Pleistocene synthems consists of a brownish calcarenite that shows high-energy shallow-water sedimentary structures, like cross and hummocky stratification. Bedding is usually sub-horizontal, but meso-scale foreset structures can be observed. Sometimes, a mollusk-rich bio-facies characterizes the calcarenites, even though in some places they are barren. Some Middle-Upper Pleistocene terraced units are made of reef carbonates, consisting of calcareous algae, serpulids, bryozoa, mollusks shells, and corals. Given these features, the depositional system of the Pleistocene terraced units can be commonly ascribed to a shallow water environment, within the shoreface water-depth (Zecchin et al., 2004).

Besides these Quaternary deposits, the coastal area of the Crotona Peninsula hosts some younger deposits. For marine deposits, younger ages can be inferred based on their elevation, which is lower than the lowest Pleistocene marine terrace in the area (MIS 3 at 9 m, see Sec. 2.3). For example, along “Spiaggia dei Gigli” (GIG in Fig. 2), low-elevation, partially stabilized sands are reported as Holocene dune deposits (ISPRA, CARG 577-Isola di Capo Rizzuto) (Fig. 2).

2.2. Tectonic setting

Terraced Middle-Upper Pleistocene units form extensive surfaces gently dipping toward the sea. These represent fossil sea floors, and they should be laterally continuous to a wide extent. However, intense disruption of such marine surfaces is often observed in the study area, mainly due to the effects of high-angle, WSW-ENE striking normal faults (Cosentino et al., 1989; ISPRA, CARG 577-Isola di Capo Rizzuto). Before the extensional regime, compressional deformation occurred in the study area. The last compressional phase in the Crotona Peninsula is recorded by gentle folding in the Piacenzian-middle Calabrian “argilla marnosa di Cutro” (Zecchin et al., 2012).

According to Capozzi et al. (2012) and Zecchin et al. (2012), seismic lines and bathymetric data offshore the Crotona Peninsula reveal other evidence of compressional tectonics. There, a bathymetric relief, known as Crotona Swell, overlies a sub-horizontal reflector emerging at the base of the swell. The classic interpretation of the Crotona Swell is a hanging-wall of an ESE-verging thrust. However, according to a new interpretation, the thrust at the base of the swell, as well as the onshore normal faults affecting the marine terraces, are attributable to a mega-landslide (Zecchin et al., 2018).

2.3. Middle-to late pleistocene marine terraces and uplift rates

Five levels of Pleistocene terraces can be observed in the Crotona Peninsula (Fig. 2). Numerous dating techniques have been applied in the Crotona Peninsula to define the age of the different marine terraces and to explore the interaction between Pleistocene sea levels and vertical movements. A summary of the literature data on elevation, the chronological constraints, and the uplift rates of these marine terraces is reported in Table 1.

In the Crotona Peninsula, the first (highest) terrace level is the most extensive. Its elevation is in the range of 161 ± 9 m a.s.l. (Fig. 2), but the inner edge reaches almost 200 m outside the study area. The age of this marine terrace has been associated to MIS 7-MIS 7.5 (Belluomini et al., 1988; Gliozzi, 1988; Nalin et al., 2020), although recent IRSL datings do not exclude ages as old as MIS 9 (Nalin et al., 2020). The second marine terrace level has its maximum elevation in the range of 88 ± 7 m a.s.l. (Fig. 2). A lower elevation is reached in the central sector of the Crotona Peninsula, where normal faults downthrow the terrace. The age of the second terrace level has been constrained by several dating methods. The presence of Senegalese fauna in the marine deposits of this terrace points to an age referable to MIS 5.5 (Gliozzi, 1988; Nalin et al., 2012). This age is also supported by OSL dating of 116 ± 10 ka (Mauz and Hassler, 2000). The MIS 5.5 age is further corroborated by recent infrared-stimulated luminescence (IRSL) dating 125 ± 7 (Nalin et al., 2020).

The third marine terrace level has an elevation mostly between 30 and 40 m, but it reaches up to 50 m NW of Le Castella. In some places, the lateral discontinuity of this terrace is the result of normal faulting (Cosentino et al., 1989). Assigning an age to the third terrace level is tricky. According to aminostratigraphy and stratigraphic correlation, it was initially thought to be referable to MIS 5.3 (Belluomini et al., 1987). However, none of the subsequent datings fall within the range of this isotopic stage. Instead, a sample dated with IRSL to 83 ± 4 ka links the lower portion of the terrace to MIS 5.1 (Nalin et al., 2020). Since a series of overlapping surfaces within the same terrace are geomorphologically recognizable (to the west of SPR locality, Fig. 2), another interpretation

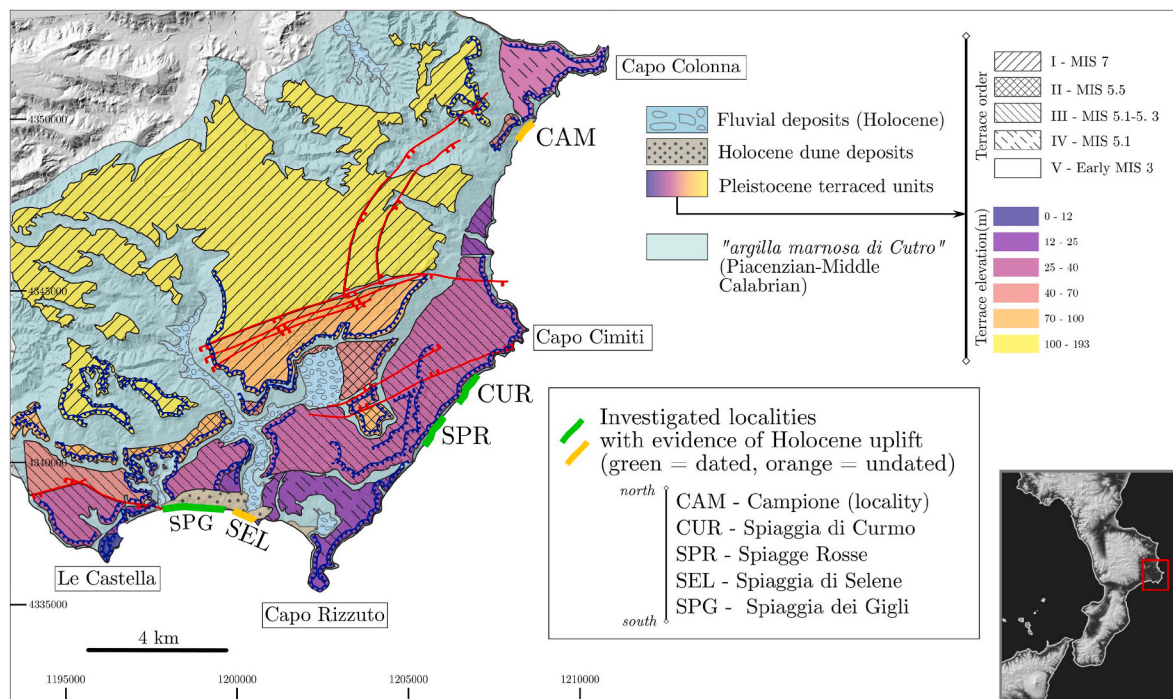


Fig. 2. Geological map of the Crotona Peninsula. Terraced Pleistocene units are coloured depending on the elevation. A superimposed pattern shows the terrace order and its age, following the most recent interpretation of Nalin et al. (2020). Localities investigated in the field campaign are also reported (green and orange lines along the coast). Red lines are normal faults; blue notched-lines are the edge of the marine terraces.

Table 1

Main data referable to the marine terraces from the Crotona Peninsula. References: a - Gliozi (1988); b - Cosentino et al. (1989); c - Mauz and Hassler (2000); d - Zecchin et al. (2004); e - Nalin et al. (2020).

Terrace Order	MIS	Age (ka)	Elevation (m)	Paleo Sea Level (m ± m)	Uplift Rate	Reference
I	7	196 ± 6	230	-4 ± 4	1.20 ± 0.06	d
I	7.5	241 ± 4	225	-5 ± 12	0.97 ± 0.21	e
II	5.5	125 ± 1	100	4 ± 1	0.78 ± 0.03	a, b, d
III	5.3	104 ± 1	65	-22 ± 15	0.84 ± 0.16	d
IV	5.1	82 ± 3	33	-30 ± 10	0.81 ± 0.15	d
IV	5.1	84 ± 2	40	-29 ± 12	0.89 ± 0.37	e
V	3	52 ± 2	8	-40 ± 12	0.96 ± 0.27	c, d
V	3	60 ± 2	6	-57 ± 12	1.02 ± 0.40	e

is possible. According to Zecchin et al. (2004), and Nalin et al. (2020), this terrace was formed between MIS 5.3 and MIS 5.1. The different recognizable terrace edges would thus be the remnants of relative sea level fluctuations within this time interval.

The fourth marine terrace level occurs along the Capo Rizzuto promontory and in the Capo Colonna area. The elevation of this marine terrace is lowest at Capo Rizzuto (22 ± 4 m), while it reaches 33 ± 10 m at Capo Colonna. Recent dating with the IRSL method to 84 ± 9 ka associates the terrace to MIS 5.1 (Nalin et al., 2020).

The fifth marine terrace level occurs in the Le Castella area at 10 ± 5 m elevation. Mauz and Hassler (2000) first dated these deposits using optical stimulated luminescence (OSL). Three samples returned an age of approximately 45–50 ka, which would associate the terrace with MIS

3. More recently, Nalin et al. (2020) dated the same terrace with OSL to an age of 64 ± 3 ka, confirming the same isotopic stage suggested by Mauz and Hassler (2000). Recently, terraced marine deposits in the area of the Strait of Messina have also been referred to MIS 3 (Antonoli et al., 2015).

3. Methods

3.1. Field measurements

Two field campaigns were performed in the study area, in April and September 2021. April campaign allowed us to perform accurate observations given the special low tide conditions (-42 cm a.m.s.l.), while most of the sampling for radiocarbon dating was performed in September. Elevation measurements were made mechanically with a tape measure. Uncertainty can be evaluated in the range of ±0.2 m. Each sea-level marker was measured with respect to the current mean sea level (MSL). The position of the latter was identifiable considering the maximum curvature of the active notch and the living algal cover at the same level. When the considered section shows no active notch, the measurement is taken from the sea level at that time. After that, the measured sea level is corrected with respect to the elevation of the currently active notch at the location closest to the studied section.

Several types of bio-geomorphological sea-level markers have been used to evaluate the paleo shoreline elevation. Erosional forms such as notches, marine sediments, and also suspended fossil riverbeds provided accurate indications of paleo coastline position, even though they were unable to provide age constraints. Dated samples were therefore collected from marine deposits related to these geomorphological features.

3.2. Radiocarbon dating

AMS radiocarbon dating was performed on carbonate material by Beta Analytic, by using ¹⁴C techniques. Conventional ages were calibrated to the MARINE20 calibration curve and a local reservoir effect

correction was applied. A value of $\Delta R = -26 \pm 70$ was used using the average of the four nearest reservoir effect estimates (<http://calib.org/marine/>). The value adopted clearly refers to calibration on the new MARINE20 curve. Calibration was performed using the MATLAB function “MatCal” (Lougheed and Obrochta, 2016).

3.3. Compilation of the database

We created a database collecting all Holocene sea level markers from Calabria. The ages were calibrated with the same global curve and local reservoir effect according to the parameters clarified above. The new calibration was not possible, however, for the samples dated by Spampinato et al. (2014), because the original paper does not report the “conventional” radiocarbon age, which is necessary to make the calibration. The datings in the original paper are reported as calibrated, but it is not clear which curve was used. Thus, one must consider that the ages of these samples may not be perfectly comparable with those of the rest of the database. We presume that any shift in age is a few tens or hundreds of years, at most.

In the database, and in this paper, we use the term “sea-level marker” as a constraint of the relative sea level (RSL) in space and time, with a clear relation to the ancient paleo-mean sea level (MSL). The second part of the definition is related to the fact that a sea-level marker may accurately represent the coastline at its time (Sea Level - SL), or it may not have this accuracy. Sometimes “sea-level markers” define a lower limit (Lower Level - LL) or an upper limit (Upper Level - UL). This concept is also critical in the interpretation of the results in terms of uplift rate. An uplift rate obtained from a LL will be a minimum estimate, while that obtained from a UL will be a maximum estimate. The vertical velocity obtained from a SL marker, on the other hand, will be the most accurate. This terminology is also associated with a color code that is consistent throughout the next figures. So, the sea level markers are coloured as follows in the graphs: SL = green, LL = blue, UL = red. We then define the term “site” as a series of sea-level markers that refer to the same coordinates. This can happen when multiple sea-level markers are found in the same vertical section. But it can also happen when the coordinate resolution cannot discern individual sea-level markers. For example, the GIG site in the database includes 10 sea-level markers. Some of them are in the same vertical section, others are too close each other so that they can be described by the same coordinates. However, the main feature of the site is related to the RSL curves produced by the GIA models. Since the site is defined by geographic coordinates, it means that a site is associated with a unique RSL curve.

3.4. GIA correction

Glacial isostatic adjustment (GIA) models are used to estimate the difference of the sea level between the current one and that at the paleo shoreline age. They depend on several inputs, primarily including the viscoelastic structure of the Earth and the deglaciation history of the polar ice caps since the last glacial maximum. We applied two widely used GIA models: ICE-6G (VM5a) and ICE-7G (VM7). Relative sea level curves calculated with these models were obtained through the open-source SELEN 4.0 software (Spada and Melini, 2019). The reliability of the curves produced by using the SELEN 4.0 freeware is ensured by tests on both real data (e.g., Vacchi et al., 2016; Liberatore et al., 2022) and synthetic data (Martinec et al., 2018). Both models showed excellent performance in approximating stable coastlines of the Western Mediterranean (Vacchi et al., 2016; Roy and Peltier, 2018) and in the Eastern Mediterranean (Liberatore et al., 2022). We also considered the ANU curve in the comparison of vertical velocities of other sectors of Calabria, because all previous works used the ANU model (e.g., Antonioli et al., 2006; Ferranti et al., 2007; Spampinato et al., 2014). The main difference between the ICE-xG and ANU curves is that the former has much smaller RSL rising rates in the late Holocene than the ANU model. This difference is due to the different deglaciation history between the two

models but also to a different lower mantle viscosity value (Peltier et al., 2015; Lambek et al., 2011). In essence, the ICE-xG curves are higher than those from the ANU model (see Sec. 4) and therefore the uplift rates calculated based on the latter are always bigger. It is worth noting that recent findings on stable coastlines indicate that ICE-xG models outperform the ANU model (Melis et al., 2018; Vacchi et al., 2016). Using the results of this model to interpret vertical tectonics may lead to erroneous conclusions.

3.5. Tectonic model

We modelled the vertical coseismic displacement of a fault in the Crotona area to test some of our hypotheses about the mechanism of the uplift. We used the Okada (1985) model for finite deformations from a rectangular source in a homogeneous elastic half-space. Our results come from a simple solver of the Okada equation (Okada, 1985) in MATLAB (Beauducel, 2022). The code provides results on a simple grid of Cartesian axes; our only modification was to show them on geographic axes. The tectonic model requires nine fault parameters as input: strike, dip angle, length, amplitude, depth of hypocenter, geographic coordinates of the fault center, total slip, rake, and opening angle (zero, in case of faults). Some of these parameters were identified using the Database of the Italian Seismogenetic Sources (DISS) (DISS 3.3.0 - DISS Working Group, 2021). Specifically, the location, geometry (strike and dip angle), fault length and width were identified in this manner. As for slip, this must be scaled to the size of the fault. For this purpose, we used the relations of Wells and Coppersmith (1994). According to empirical equations, the moment magnitude (M_w) is related to both the mean slip [S (m), Eq. (1) and Eq. (2)] and the total rupture area [RA (km^2), Eq. (3)]. Arranging Eq. (2) and Eq. (3) gives the relationship between average slip and rupture area in Eq. (4).

$$M_w = 6.93 + 0.82 \times \log_{10} S \quad (1)$$

$$S = 10^{\frac{M_w - 6.93}{0.82}} \quad (2)$$

$$M_w = 4.07 + 0.98 \times \log_{10} RA \quad (3)$$

$$S = 10^{\frac{(4.07 + 0.98 \times \log_{10} RA) - 6.93}{0.82}} \quad (4)$$

4. Results

4.1. Field evidence and radiocarbon dating

Traces of past sea levels were found on three of the five investigated sites (Fig. 2), where carbonate samples were collected for radiocarbon dating. Starting from south, and moving north-eastward (Fig. 2), we present below a description of the investigated sites. Further details can be found in Figs. S1–S6 in the Supplementary Material.

4.1.1. Spiaggia dei Gigli (GIG)

Spiaggia dei Gigli is a long sandy beach between Le Castella and Capo Rizzuto (Fig. 3A). Numerous lines of evidence of a relative sea level higher than the present one has been observed in this locality. Along the eastern sector of the beach, there are large blocks of Upper Pleistocene calcarenite, fallen down from the cliff, lying and embedded in the current beach sediment (Fig. 3). These blocks show a wave notch about 1 m above the current MSL. The lateral continuity of the fossil notch is extensive. Often, it can be found on all sides of the blocks, forming notch-mushroom morphologies (Fig. 3C–D). The vertical width of the notch reaches more than 70 cm, while the depth is about 30 cm. Moreover, the notch is in some places associated with a wide abrasion platform, which can reach more than 3 m in horizontal width (Fig. 3B).

In addition to the notch, there are also sandy marine deposits that are clearly referable to a RSL higher than the current sea-level. These deposits were studied through dedicated sections crossing the beach zone

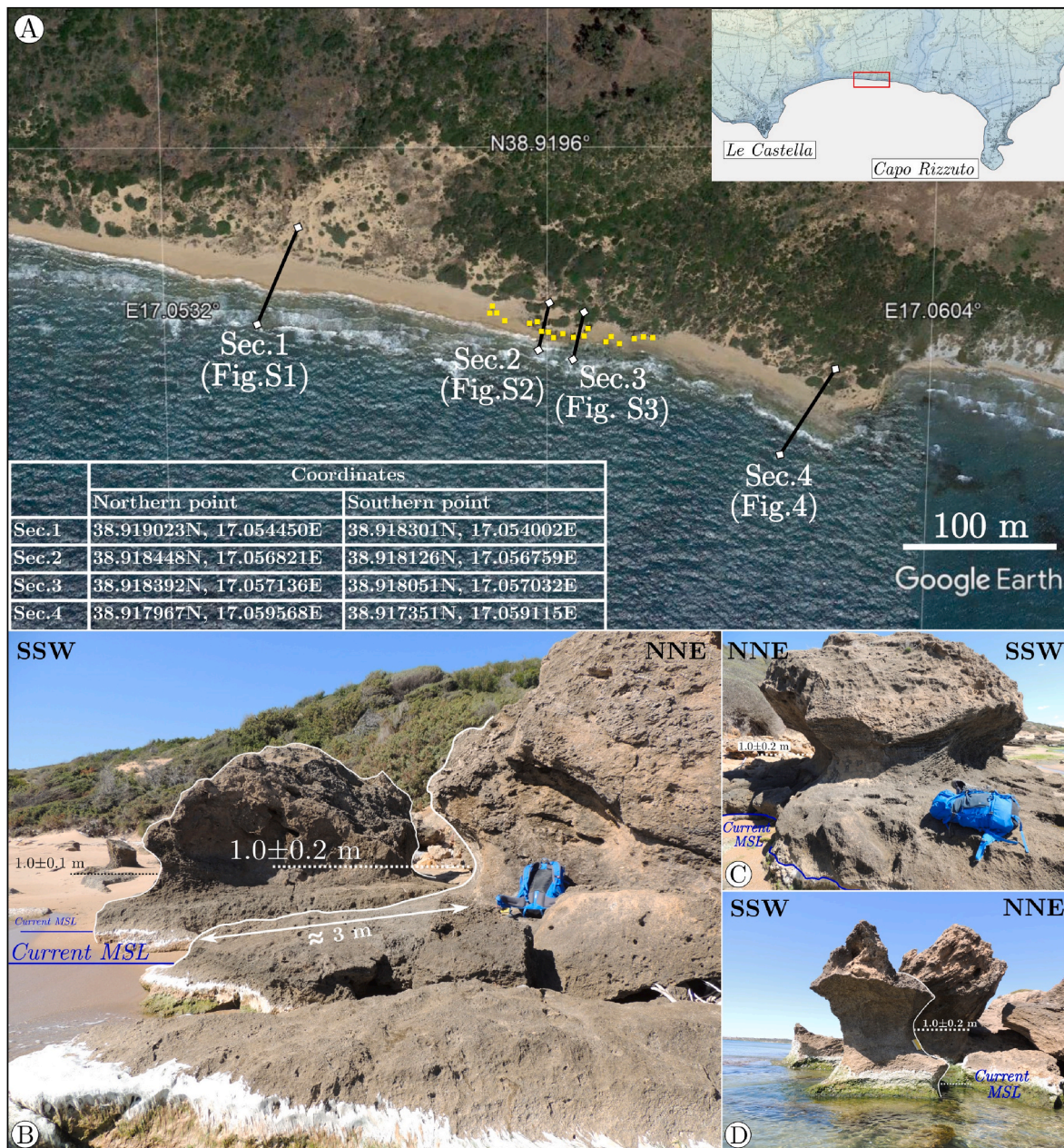


Fig. 3. | Outcrops in Spiaggia dei Gigli. A) Position of the studied sections. Yellow squares are blocks of Upper Pleistocene calcarenites hosting uplifted notches (B). C-D) mushroom-type fossil notches close to Sec.2 line. Special seasonal low-tide condition (≈ 40 cm below the m.s.l.) produced the white stripe in the picture made of dead algae.

(Fig. 3A).

In Section 1 (Fig. S1, see Fig. 3 for location), there is a cemented sand bank in the innermost part of the beach. It contains numerous shells or fragments of cardites, mainly *Cerastoderma* sp. These mollusks have often been used as Holocene and Pleistocene sea-level markers, since they live in water depths between 0 and -2 m in brackish marginal-marine lagoons (Antonioli et al., 1999; Lambeck et al., 2004 and references therein; Lambeck et al., 2011). Moreover, the organization of these sediments in thin layers allows us to exclude that the deposition occurred by storm events or other high energy processes. On top of this marginal-marine deposits there is a cemented sandy layer rich in *Helicidae* remains, pointing to a terrestrial environment. Moving up section, cross-bedding structures characterize these terrestrial deposits, which are referable to aeolian sands as dune cords (aeolianites). Finally, up section, loose sandy sediment of the active dune covers these aeolian

fossil dunes. The highest *Cerastoderma* sp. In the lagoonal marginal-marine deposits was sampled as GIG 1 for radiocarbon dating. Its elevation, between 2.1 and 2.5 m a.m.s.l. Represents a lower constraint for the shoreline (which must have been above that level). The resulting age is 7099–6621 cal Yr BP. In the aeolianites, on the other hand, a sample of *Helicidae*, taken as GIG 2 at 2.5–2.9 m a.m.s.l. Yielded an age of 2698–2578 cal Yr BP.

In Section 2 (Fig. S2), a mushroom-like notch is developed at 1.0 ± 0.2 m a.m.s.l., around an Upper Pleistocene calcarenite block. At the base of the notch, covered by the modern sandy sediment, there is a well-cemented sandy deposit, organized in cm-thick strata. The lower portion is a cobble conglomerate of calcarenites and *Cerastoderma* sp. Shells. Given the distribution of the sediment, it is likely that it was the deposit related to the same sea level as the notch. A shell of *Cerastoderma* sp. Was sampled as GIG 3a (3237–2769 cal Yr BP). We also sampled a calcareous

encrustation made of algae and serpulids as GIG3b. It was attached on the notch, just below the maximum curvature (Fig. S2). It yields an age of 2610–2090 cal Yr BP.

Section 3 (Fig. S3) shows one more notch of the same 0.9–1.1 m a.m. s.l. Coastline, which produces a mushroom-shaped block. It is surrounded by a consolidated marine deposit made by large pebbles and remains of large mollusc shells. Some lithodome boreholes can be observed on it. The radiocarbon ¹⁴C dating of a pectinide fragment (GIG 7a) provided an age of 7173–6715 cal Yr BP. In a niche on the notch, a calcareous algal encrustation was taken (sample GIG 7 b) and dated to 4841–4385 cal Yr BP.

Section 4 (Fig. 4) shows similarities with Section 1. In this section, a well cemented unit made of conglomerate, rich in *Cerastoderma* sp. Shells, crops out in the beach zone, just below the modern beach deposits. Close to the current sea level, the stratification slightly dips seaward by a few degrees. It becomes sub-horizontal as it approaches the dune zone. The bedding and sedimentological characteristics of the conglomerate are typical of a foreshore and beach environment. Its

distribution at the base of the notches also supports its proximity to palaeo sea level. However, the presence of *Cerastoderma* sp. Allows us to hypothesise the presence of a lagoon environment close to and probably connected with the sea. Going upsection, the conglomerate layers give way to weakly cemented sands, similar to the sandy unit of Section 1. Thin layers of fairly cemented sand host fragments of *Cerastoderma* sp. Up to a maximum elevation of 2.5 m. Above that, sedimentary structures associated with an aeolian environment become prevalent and the first fossils of terrestrial gastropods appear at 3.3 m elevation. GIG8a and GIG8b are samples of the uppermost *Cerastoderma* sp. Shell and the lowest continental gastropod (*Helicidae*), respectively. Their ages are 7058–6579 cal Yr BP for the former and 5317–5051 cal Yr BP for the latter.

4.1.2. Spiaggia di Selene (SEL)

In the same gulf between Le Castella and Capo Rizzuto, a little to the east of Spiaggia dei Gigli, Spiaggia di Selene is developed at the mouth of a stream. Its riverbed is directly dug into the “argilla marnosa di Cutro”.

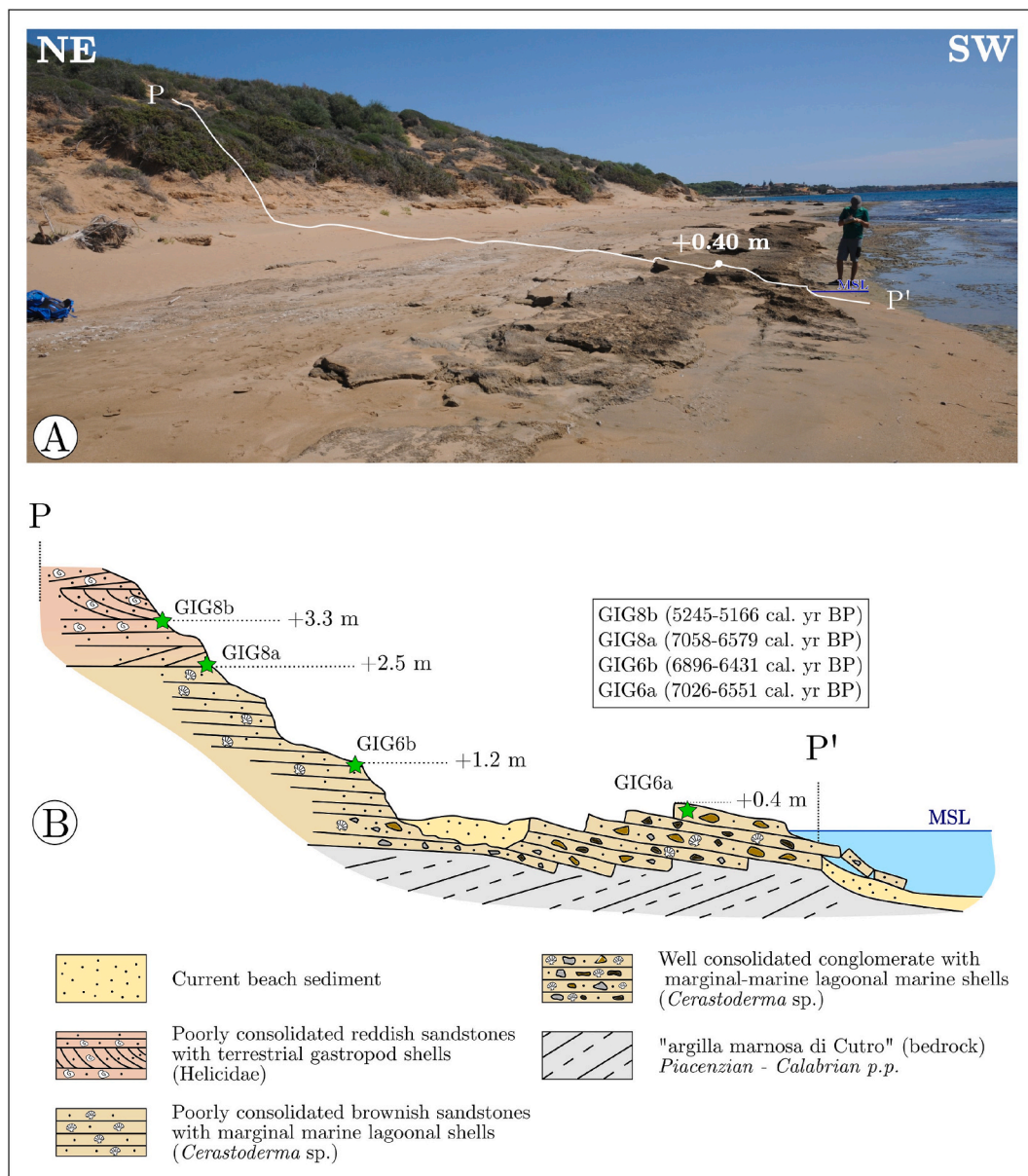


Fig. 4. Spiaggia dei Gigli, Section 4. A) Picture of the marine sediments outcropping in Section 4; B) Schematic geological cross-section of the study site with location of the 14C dated samples.

The equilibrium of the watercourse with its current base level is evidenced by the small alluvial plain that develops around the stream. This small alluvial plain is located at sea-level and is overlain by loose deposits of beach sand and coastal dune. At approximately 1.8 m a.m.s.l., a consolidated sandy unit overlies, through a sharp angular unconformity, the “argilla marnosa di Cutro”. These consolidated sands exhibit structures typical of aeolian transport and are completely barren of fossils. However, their lithostratigraphic position, the lithological characteristics, and the proximity to the Spiaggia dei Gigli, allow us to correlate this deposit to the terrestrial sandy unit that we were able to date through samples GIG 2 and GIG 8a. The unconformity between the “argilla marnosa di Cutro” and the overlying aeolianites clearly traces a paleo-riverbed like the currently active one. The fossil riverbed is in disequilibrium with the current base level, as it is cut by the currently active river channels (Fig. S4).

4.1.3. Spiagge Rosse (SPR)

This is the site already described by Pirazzoli et al. (1997). Along Spiagge Rosse beach (Fig. S5), a conglomerate beachrock crops out from the current sandy sediment. The beachrock is formed by several slabs dipping towards the sea with inclinations between 8° and 11°. The lithology of the deposit is variable (Fig. S5B). At the base of the slabs there are conglomerate facies with large pebbles (10–30 cm) and many remains of large molluscs. In the upper part, on the other hand, a calcarenitic sediment prevails. The boundary between the two facies is not always clear. Often, they can be found interfingering with each other in patterns that are not easy to schematize. There are also laminated carbonate concretions that cover the top of the beachrock and some cavities inside it (Fig. S5C). These consist entirely of calcareous algae and serpulids, forming small carbonate mounds or coating the rock surface. The sample dated by Pirazzoli et al. (1997) was taken from one of these features. We also dated these encrustations (sample SPR2, 4251–3735 cal Yr BP). We also collected SPR1, a shell of *Patella* sp. From the highest point of the beachrock (1.3 ± 0.2 m a.m.s.l.), which yielded an age of 3020–2542 cal Yr BP (Fig. S5D).

Beachrocks are known to have a submerged part and an emerged part. In the next site (Spiagge di Curmo, Section 4.1.5), for example, we studied a currently active beachrock that reaches up to 60 cm a.m.s.l. We

believe that the portion of beachrock sampled at Spiagge Rosse is the submerged portion, as it is commonly covered by algal and serpulids encrustations that can only live below the MSL.

4.1.4. Spiaggia di Curmo (CUR)

Spiaggia di Curmo is developed at the foot of a cliff formed by Upper Pleistocene calcarenites resting on top of the clays of the “argilla marnosa di Cutro”. This stratigraphic setting has important hydrogeological implications, as it determines the formation of a freshwater aquifer within the Upper Pleistocene calcarenites. In the Spiaggia di Curmo, freshwater comes out from the calcarenites at the base of the cliff, then crosses the beach zone flowing into the sea. The mixing of freshwater, rich in calcium carbonate, and seawater within the beach sediment promotes the precipitation of calcite in the pores of the sediment and the formation of beachrocks (e.g., Vousdoukas et al., 2007; Mauz et al., 2015). Along the beach of Curmo, in correspondence with freshwater flows, it is possible to observe an active beachrock, whose elevation does not exceed 60 cm a.m.s.l. (Fig. S6). The grain size, detrital grain composition, their colour, and especially the mollusk remains of the beachrock are identical to that of the modern unconsolidated beach sands. Both the beachrock and the beach sand are rich in *Tellinidae* and *Veneridae* shells. The ¹⁴C dating of a *Tellinidae* shell (sample CUR1) from the beachrock, returning a Post 1950 age, confirms the observation we previously made on the beachrock and the current beach sands.

In addition to sea-level markers developing at the current sea-level, other markers related to a higher RSL were found on the same beach. A well-cemented cliff breccia and conglomerates, made by meter-scale calcarenite blocks, with a sandy or coarser matrix rich in marine shells (Fig. 5), were found on the Curmo beach. One of the calcarenite blocks retains traces of a notch at about 1.2–1.3 m a.m.s.l. At the notch elevation, a trochid shell (CUR2, see Fig. 5A) was collected from the conglomerate. It returned a ¹⁴C age of 3755–3282 cal Yr BP. Slightly lower than the notch at 1.2–1.3 m a.m.s.l., attached to the conglomerate, calcareous encrustations made by algae and balanids were found (Fig. 5B). A balanid shell (sample CUR3) returned a ¹⁴C age of 2600–2076 cal Yr BP. The presence of balanids itself is not an indication of sea level, as these organisms can also live in the emerged spray zone (Labrel and Labrel-Deguen, 1996). However, the association with the

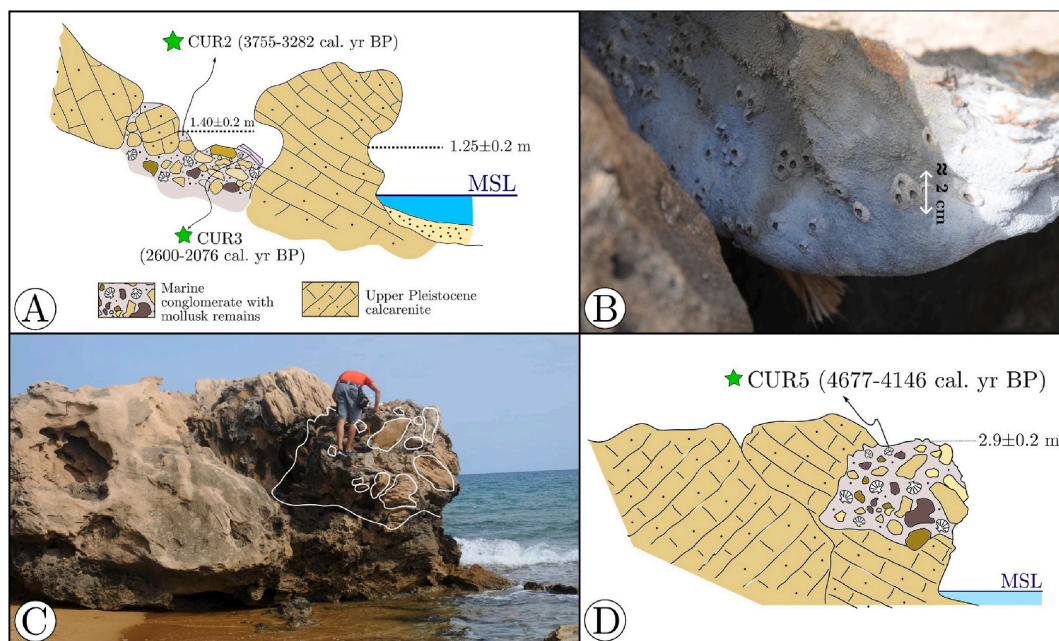


Fig. 5. Spiaggia di Curmo: A) sketch showing the position of CUR2 (trochid) and CUR3 (balanid) sea level markers; B) Detail of the balanids (sample CUR3) and calcareous algae encrustations on a calcarenite block of the cliff breccia; C) Picture showing the cliff breccia with marine conglomerates cut by an abrasion platform on top; D) Sketch of the outcrop described in C, showing the position of sample CUR5.

calcareous algae suggests that these organisms lived at or slightly below MSL.

Along the same beach sector, marine conglomerate with a small abrasion platform was found at an elevation of up to 2.9 m (Fig. 5C). Several shells of *Patella* sp. (sample CUR5) were found on this abrasion platform. CUR5 yielded a ^{14}C age of 4677–4146 cal Yr BP.

4.1.5. Località campione (CAM)

Although no dating was possible for this site, this locality provides the northernmost evidence on the Crotona Peninsula of a higher relative sea level (Fig. 2). Similar to Spiaggia di Selene, a suspended riverbed was found between 1.7 and 3.3 m higher than the currently active riverbed. Different from the Spiaggia di Selene site, in this locality, a 1.5 m thick fluvial deposit made by well-rounded pebbles unconformably overlies the “argilla marnosa di Cutro”.

4.2. Holocene uplift rates and vertical movements history in the Crotona Peninsula

To define the uplift rates and the vertical movements of the Crotona Peninsula, ages of dated samples were plotted against RSL curves calculated with GIA models (Fig. 6). All samples fall above the RSL predicted by GIA models. This means that a tectonic uplift component must be responsible for the current position of the sea level markers considered in this work. The calculated uplift rate for each sea level marker is given in Table 2.

4.3. Holocene vertical velocity fields in Calabria

In this section, the sea-level markers from other Calabria localities (see Fig. 1) are compared with the corresponding RSL curves (Fig. 7). In all the localities we are comparing, the sea-level markers fall above the sea-level prediction of the GIA models. Only for the Briatico locality (BRI, Fig. 7) there is no evidence of uplift. The details of the obtained vertical velocities can be found in Table 3 and Fig. 10.

5. Discussion

5.1. Comparison between late Pleistocene and Holocene uplift rates and other locations in Calabria

The comparison between Holocene and late Pleistocene uplift rates have two important characteristics: 1) sea-level markers with ages of 6–7 ka perfectly match the most reliable estimates of late Pleistocene uplift rates (Fig. 8); 2) sea-level markers with ages of 5–2 ka are slower than late Pleistocene uplift rates.

The slower uplift rates in the younger markers could lead to the conclusion that the uplift rate of the Crotona Peninsula has decreased over time. But the slower uplift could be simply related to a mathematical issue concerning the calculation of the uplift rate. Because age is in the denominator in this calculation, the more the denominator decreases, more the sensitivity of the uplift rate to discrete uplift events increases. Fig. 9 shows a graph for better understanding this concept. Suppose we have a series of sea level markers with ages between 100 and 10,000 yrs at similar elevation, about ± 1 m one from each other. Suppose next that there is a discrete increase in uplift so that, within a short time (\ll age of the marker), all coastlines acquire the same increase in uplift. Recalculating the uplift rate after that event, one would get higher uplift rates, although the increase in uplift rate would be different, depending on the age of the considered coastline. Younger coastlines would acquire a much higher increase in uplift rate, while older coastlines would acquire a small or no increase in uplift rate. For example, considering a 1000-year-old coastline affected by a discrete uplift of 0.2 m, it would acquire 0.2 mm/yr of uplift rate. In contrast, a coastline with an age of >5 –6 kyr, affected by the same increase in uplift, would experience either a little or no change in uplift rate. That is, younger shorelines are much more sensitive to uplift increase than shoreline a few thousand years older. The transition between stable and unstable uplift rates would appear to occur at around 5–8 kyr (Fig. 9). It could be said that uplift rates evaluated for shorelines younger than 5 ka are estimates on a short term, whereas shorelines older than 8 ka are more likely reflect the long term uplift rate. Therefore, in the Crotona Peninsula, where Holocene sea-level markers of 2–5 ka show lower uplift rates with respect to older markers, it could be assumed that shorelines of this age lack a certain amount of uplift. A future, discrete uplift event of ca. 50 cm affecting the Crotona Peninsula would balance of all the Holocene and even late Pleistocene uplift rates.

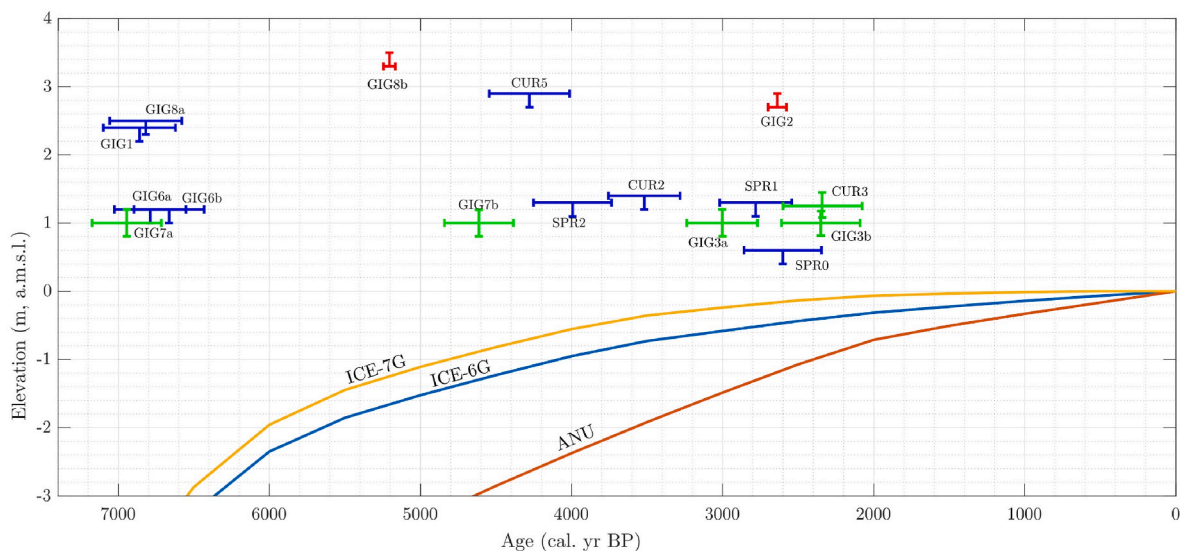


Fig. 6. Relation between sea-level markers in the Crotona Peninsula and RSL curves from GIA modeling. Each point represents a sea level marker; different colours are for the different relationship with the paleo-sea level following what reported in Section 3.3 (Compilation of the database). Green markers represent a sea level (SL), blue markers a lower level (LL), while red markers are continental samples dating an upper level (UL).

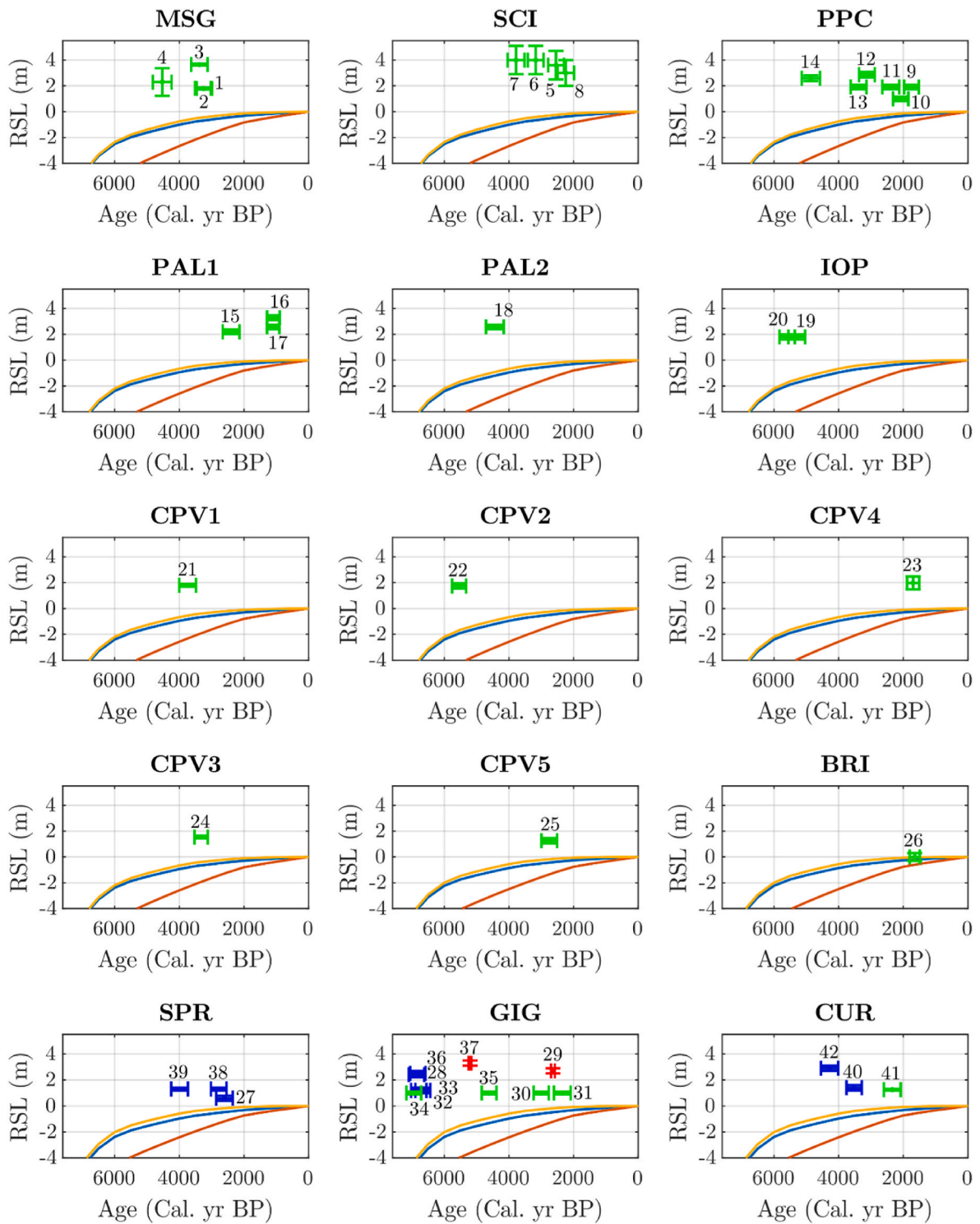


Fig. 7. | RSL curves vs sea-level markers in Calabria. Markers of each site are plotted against the RSL curve associated to the site’s coordinates. Colour scheme is the same as for Fig. 6. Numbers within the graphs refer to “Marker ID” column in Table 2 and Table 3.

By the same reasoning, the variability of the uplift rate in different parts of Calabria can be partly explained with the graph of Fig. 10. In this figure, the differences in uplift rates can be examined in space and time, where all the uplift rates are plotted with the corresponding age. Sea level markers are also coloured according to the distance from the Messina Strait (geodetic distance, in km). Areas within 20 km from the Messina Strait (dark blue, blue, and green dots in Fig. 10) show uplift rates averaged over short time periods that are greater than those averaged over longer time periods. In contrast, the Capo Vaticano area

shows a similar trend of time-averaged uplift as the Crotona Peninsula. Considering the sensitivity of the calculated uplift rate to the averaging time period, one could interpret these differences through a deficit or surplus of recent uplift. The coastlines of the Messina Strait may have acquired a discrete uplift pulse in recent times, so they are not yet rebalanced with the stable uplift rate value calculated over a longer term. The numerous active faults roughly parallel to the coast are ideal candidates for generating some amount of discrete uplift at the surface (Ferranti et al., 2007, 2017; Spampinato et al., 2014). The Capo

Table 2

Holocene uplift rates of the Crotona Peninsula sea level markers. "Marker ID" column is for reference in Fig. 7; "Marker" column is for reference in Fig. 6. See Section 3.3 (Compilation of the database) for colour coding.

Marker ID	MARKER	ICE-7G velocity (mm/yr)	ICE-6G velocity (mm/yr)	ANU velocity (mm/yr)
27	SPR0	0.30 ± 0.03	0.41 ± 0.05	0.68 ± 0.07
28	GIG1	0.93 ± 0.03	0.98 ± 0.04	1.46 ± 0.05
29	GIG2	1.09 ± 0.03	1.21 ± 0.03	1.48 ± 0.03
30	GIG3a	0.42 ± 0.04	0.53 ± 0.04	0.84 ± 0.07
31	GIG3b	0.48 ± 0.06	0.60 ± 0.07	0.85 ± 0.11
32	GIG6a	0.73 ± 0.03	0.78 ± 0.03	1.24 ± 0.05
33	GIG6b	0.69 ± 0.03	0.74 ± 0.03	1.16 ± 0.04
34	GIG7a	0.75 ± 0.03	0.80 ± 0.03	1.31 ± 0.04
35	GIG7b	0.42 ± 0.02	0.50 ± 0.03	0.87 ± 0.05
36	GIG8a	0.93 ± 0.03	0.98 ± 0.04	1.45 ± 0.05
37	GIG8b	0.88 ± 0.01	0.96 ± 0.01	1.33 ± 0.01
38	SPR1	0.54 ± 0.05	0.66 ± 0.06	0.95 ± 0.09
39	SPR2	0.47 ± 0.03	0.57 ± 0.04	0.93 ± 0.06
40	CUR2	0.51 ± 0.04	0.61 ± 0.04	0.96 ± 0.07
41	CUR3	0.59 ± 0.07	0.71 ± 0.09	0.95 ± 0.12
42	CUR5	0.85 ± 0.06	0.94 ± 0.06	1.31 ± 0.09

Table 3

Uplift rates in the Tyrrhenian Calabria according to the different GIA models. See Fig. 1 for site location and Fig. 7 for checking the distance of the sea level markers relative to the modelled RSL curves. See Section 3.3 for color code.

Marker ID	SITE	ICE-7G velocity (mm/yr)	ICE-6G velocity (mm/yr)	ANU velocity (mm/yr)
1	MSG	0.69 ± 0.05	0.76 ± 0.06	1.14 ± 0.09
2	MSG	0.69 ± 0.05	0.76 ± 0.06	1.14 ± 0.09
3	MSG	1.22 ± 0.10	1.29 ± 0.10	1.68 ± 0.14
4	MSG	0.75 ± 0.05	0.80 ± 0.05	1.22 ± 0.08
5	SCI	1.51 ± 0.16	1.60 ± 0.17	1.91 ± 0.20
6	SCI	1.39 ± 0.11	1.47 ± 0.12	1.84 ± 0.15
7	SCI	1.23 ± 0.09	1.30 ± 0.10	1.70 ± 0.13
8	SCI	1.42 ± 0.18	1.51 ± 0.20	1.79 ± 0.23
9	PPC	1.16 ± 0.17	1.25 ± 0.19	1.50 ± 0.23
10	PPC	0.55 ± 0.07	0.64 ± 0.08	0.91 ± 0.12
11	PPC	0.89 ± 0.11	0.98 ± 0.12	1.28 ± 0.16
12	PPC	1.05 ± 0.09	1.13 ± 0.09	1.49 ± 0.13
13	PPC	0.71 ± 0.06	0.78 ± 0.06	1.17 ± 0.09
14	PPC	0.80 ± 0.05	0.85 ± 0.05	1.27 ± 0.08
15	PAL1	0.99 ± 0.12	1.08 ± 0.13	1.38 ± 0.17
16	PAL1	3.03 ± 0.66	3.13 ± 0.69	3.38 ± 0.74
17	PAL1	2.37 ± 0.50	2.47 ± 0.52	2.71 ± 0.57
18	PAL2	0.79 ± 0.05	0.85 ± 0.06	1.26 ± 0.08
19	IOP	0.62 ± 0.03	0.67 ± 0.03	1.09 ± 0.06
20	IOP	0.63 ± 0.03	0.68 ± 0.03	1.09 ± 0.05
21	CPV1	0.63 ± 0.05	0.70 ± 0.05	1.10 ± 0.08
22	CPV2	0.62 ± 0.03	0.66 ± 0.03	1.08 ± 0.04
23	CPV4	1.21 ± 0.15	1.31 ± 0.16	1.56 ± 0.19
24	CPV3	0.58 ± 0.04	0.66 ± 0.04	1.04 ± 0.07
25	CPV5	0.52 ± 0.05	0.62 ± 0.06	0.95 ± 0.09
26	BRI	0.02 ± 0.00	0.13 ± 0.01	0.37 ± 0.04

Vaticano area would instead have a small uplift-rate deficit that could be filled by a future discrete uplift event. Some points show anomalous uplift velocities compared to the average of the area. The vertical velocity of samples D5b and D5c (Fig. 10) is offscale likely because storm waves or tsunamis (Ferranti et al., 2017) have carried marine remains to elevations well above the paleo-MSL. Ferranti et al. (2017) point to the magnitude 6.3 earthquake of 853 AD as the responsible tsunamigenic event. Also, marker CV5 is well above the average for its area. The authors (Spampinato et al., 2014) do not explain its anomalous elevation with respect the samples from the same coastline. In our interpretation, we cannot rule out that it may be either affected by carbon contamination, or its elevation may include a component of unrestored coseismic dislocation. Finally, BRI, the most recent sea level marker, brings with it some interesting information, as it has not been displaced from its original position. Its velocity, which is not exactly zero, is due solely to

the prediction of the GIA model, which associates the age of the sample with a slightly lower RSL than the current one. This marker indicates that there was virtually no uplift in ca. 1.6 kyr in this area. Our result is therefore different from the value of 0.65 mm/yr obtained by Anzidei et al. (2013). The difference is solely due to the adopted GIA model. The RSL curve adopted by Anzidei et al. (2013) was fitted with the ANU model (Fig. 7), which is much lower than the ICExG curves that we consider more reliable (See Section 3.4).

5.2. The Crotona Peninsula Holocene uplift history

The sea level markers in Fig. 11 can be organized into two main clusters. A first cluster includes the oldest sea level markers (GIG 6a, GIG 6 b, GIG 1, GIG 7a, GIG 8a), having an average age of 6815 cal Yr BP. Given their overlapping ages and similar elevations, these sea level markers could be related to a single paleo-coastline. We define this paleo-level as CL1. However, the precise elevation of this ancient shoreline cannot be precisely defined, as individual elevations range from 1.2 to 2.4 m. Moreover, apart from GIG 7a, the other markers do not precisely mark the sea level but rather a level that was, albeit slightly, below it. The age of GIG 7a, however, is possibly not reliable. Looking at Fig. S3, we note that the sample was taken from a deposit embedded in the notch at 1.0 ± 0.2 m elevation. That is, the deposit from which GIG 7a was derived must necessarily have been contemporary with or older than the notch. But this notch marks the coastline that we refer to the second cluster of sea-level markers, which we call CL2. This second cluster includes GIG 3 b, GIG 3a, CUR 3, SPR 1, SPR 0 and has an average age of 2615 cal Yr BP. We therefore believe that GIG 7a, which is a pectinid fragment in a marine conglomerate, was resedimented in a coastal environment referred to the second cluster of sea-level markers (CL2 coastline). However, a number of samples remain excluded from CL1 and CL2, as they are between these two main coastlines. Understanding the position of the RSL in between CL1 and CL2 is more complex, although there are several equally valid interpretations to explain them.

The main issue concerns the sea level marker CUR 5 at 2.9 m. This sample would indicate that at 4279 cal Yr BP, the RSL must have been at least at that elevation. But at about the same age there is GIG 7 b, at a much lower elevation, compatible with CL2 coastline (1.0 ± 0.2 m). We rule out the possibility that this is the same coastline subsequently displaced, which would require a tectonic element capable of producing 1.9 m of throw in about 4.2 kyr. A fault with these characteristics would be a regional structure with a clear morphological expression that instead is not detectable either in the field or from digital elevation models. The age of at least one of the two sea level markers is therefore incorrect. CUR 5 is a *Patella* sp. Shell that could be affected by a re-sedimentation or contamination problem. For example, it could have arrived at that elevation with some storm waves. Or the age of GIG 7 b could be wrong: this, however, is an encrustation of calcareous algal and serpulid, sessile organisms that were taken directly from inside the notch of CL2. GIG 7 b therefore cannot have been resedimented, but may have been affected by carbon contamination. On the other hand, this encrustation should return an age like that of the CL2 group, i.e., 2615 cal Yr BP. The mismatch strengthens the contamination hypothesis, but it could also be that the CL2 notch at the age of GIG 7 b (4613 cal Yr BP) was already active.

Since we cannot find a solution, we must necessarily work out two different hypotheses about the location of the intermediate coastline between CL1 and CL2.

1. The correct information is from CUR 5, so GIG 7 b is affected by contamination.
2. The correct information is that of GIG 7 b, and therefore CUR 5 is affected by re-sedimentation or contamination.

Each of these hypotheses provides different constraints on the

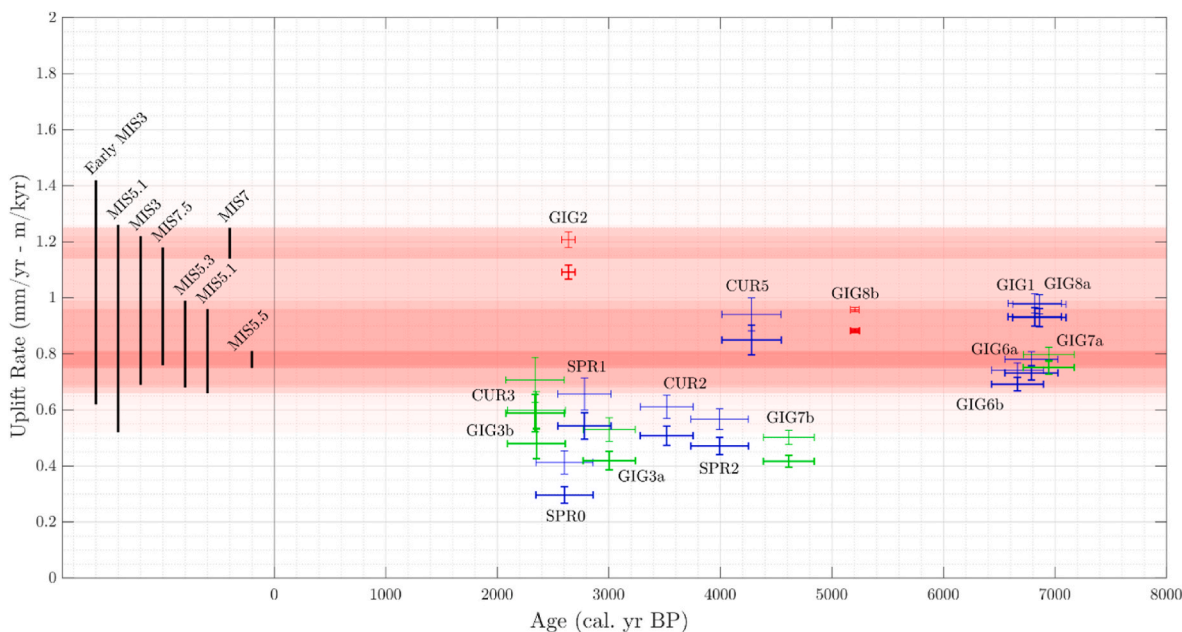


Fig. 8. Graph comparing middle-to-late Pleistocene (horizontal bars in red) and Holocene uplift rates (errorbars) in the Crotone Peninsula. In the window on the left, black vertical bars highlight middle-to-late Pleistocene vertical uplift rates: for each, the marine isotope stage (MIS) from which the estimate is derived is shown. Middle-to-late Pleistocene uplift rates show rather wide variability, but mostly cluster around values of 0.7–1.0 mm/yr. The uplift-rate estimate of ca. 0.8 mm/yr resulting from the marine terrace referred to MIS 5.5 falls within this range. This terrace was dated with several methods (Table 1), and therefore represents a higher quality uplift-rate estimate with respect to the other marine terraces. On the right side of the graph, the Holocene vertical velocities are shown. Bold uplift rate error bars were evaluated by using ICE-7G (VM7) GIA model, while thin uplift rate error bars were obtained from ICE-6G (VM5a) GIA model. The colour of the error bars follows the colour code in Section 3.3.

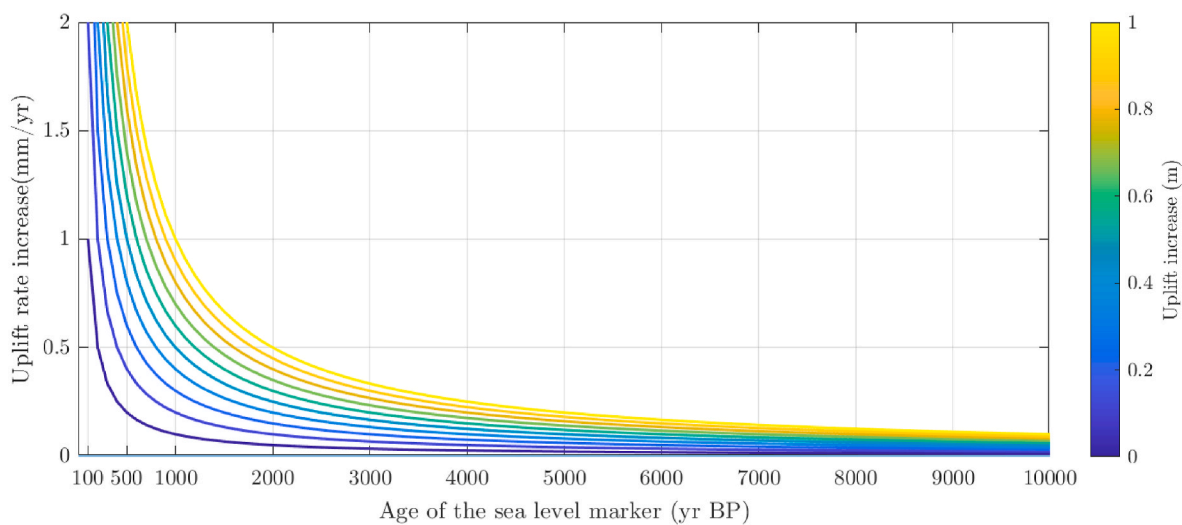


Fig. 9. | Uplift rate sensitivity to discrete uplift events. The figure shows how much the average uplift rate of a coastline of a certain age increases as a result of a discrete increase in uplift.

shoreline position around 4–5 ka. Therefore, a different uplift path must be analyzed for each hypothesis. In Fig. 11, we have attempted to draw two of the infinite paths that can be defined by the constraints from CUR 5 and GIG 7 b. To make these reconstructions reasonable, however, it must also be considered that uplift occurred almost homogeneously throughout the study area. This limitation is compatible with the geology of the area and the arrangement of sea level markers: the markers are located within a few kilometers of each other, and no significant tectonic features were detected between their locations. The same CL2 coastline elevation at the three different localities (GIG, SPR and CUR) allows us to assume the absence of significant tilting or disarticulation of the uplifting block. Uplift path 1 (UP1 – Fig. 11) - In this simulation, the

information from CUR 5 is considered valid, not that from GIG 7 b. The first uplift constraint is given by the continental sample GIG 8 b at 5305 cal Yr BP. Between the age of CL1 (6789 cal Yr BP) and GIG 8 b, the sea level rose 2.1 m. But sample GIG 8 b was sedimented in the terrestrial environment and is only 1.5 m above CL1. Therefore, there must have been a minimum uplift of 0.6 m in the meantime. However, the uplift could have been even up to 1.6 m depending on the paleo-depth of GIG 6 b. This is the uplift constraint value obtained between 6789 and 5205 cal Yr BP; above this uplift value, the vertical distance between GIG 8 b and the other sea-level markers would no longer be respected. The second uplift constraint is CUR 5 at age 4278 cal Yr BP. This sample was supposed to be at or just below sea level at its age. Assuming it was at sea

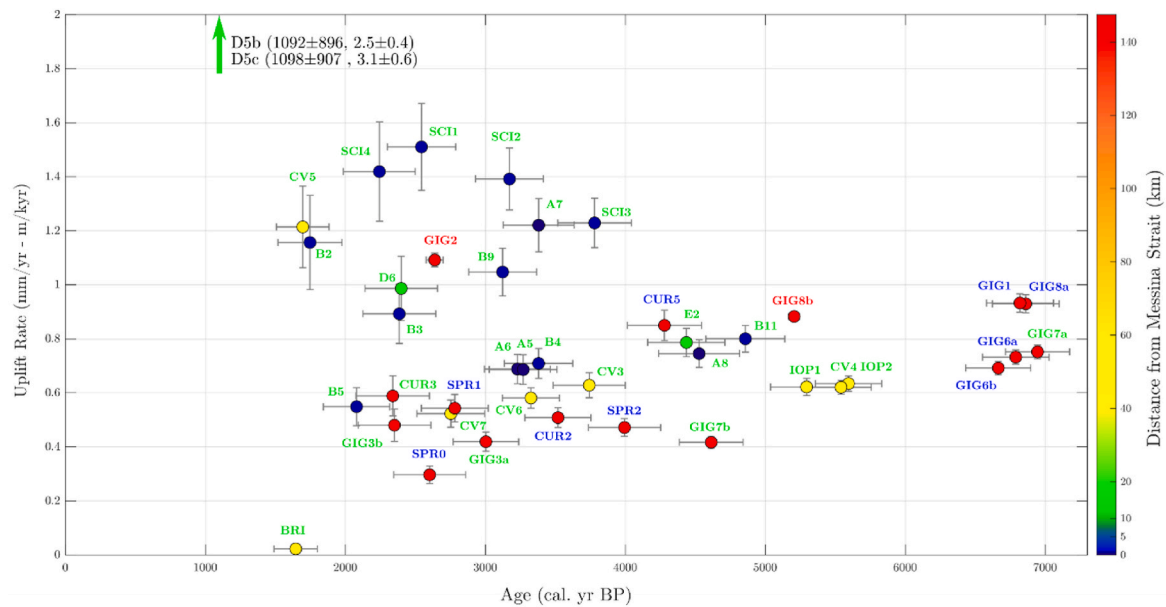


Fig. 10. | Comparison of Holocene uplift rates obtained for all the Holocene sea level markers in Calabria. The colour of the points depends on the distance from the Messina Strait. The colour of the marker labels depends on the original position of the marker relative to the pMSL: green, the marker is representative of the pMSL, provides an accurate measure of the uplift rate. Blue, the marker is below the pMSL, it provides a minimum estimate of the uplift rate. Red, the marker is above the pMSL, it provides a maximum estimate of the uplift rate.

level, we would have at least 0.6 m of uplift during this second time interval (5205–4768 cal Yr BP). Then, at 3003 cal Yr BP, the activation of the CL2 coastline constrained by sample GIG 3a. GIG 3a is located 2.3 m vertically below GIG 8 b. For the distances of the sea-level markers to be respected, and considering the sea-level rise of 0.5 m between CUR 5 and GIG 3a, we have to assume an uplift of 2.8 m between 4268 and 3003 cal Yr BP. The sea level remains stable in CL2 until 2300 cal Yr BP. Then a rapid uplift event of about 1.1 m may have occurred, leading to the abandonment of CL2 (details of this will be discussed later). We thus arrive at the current arrangement of sea-level markers. According to this reconstruction, in the period between CUR 5 and GIG 3a, the RSL was between 2.9 and 1 m a.m.s.l. This reconstruction is consistent with constraints for the sea-level markers CUR 2 and SPR 2, since sea level must have been at their elevation or slightly higher.

Uplift path 2 (UP2 – Fig. 11) - In this simulation, the information from GIG 7 b is considered valid, but not that from CUR 5. The uplift path remained unchanged until 4613 cal Yr BP. At that point, RSL was established at CL2. This coastline would remain active from 4613 to 2300 cal Yr BP, even though the sea level rose by about 0.8 m during that time period. It could be that a small amount of uplift kept the CL2 shoreline active, but it could also be that the notch migrated vertically along with sea level. This hypothesis cannot be dismissed, as 0.8 m of sea level rise in 2300 years is a low rate, consistent with the rate of notch erosion (Antonoli et al., 2015). In the period between GIG 7 b and GIG 3a, the RSL always remained at 1 m a.m.s.l. CUR 2 and SPR 2 are thus sea level markers of the CL2 coastline.

Given the limited number of constraints, these reconstructed uplift histories are affected by many uncertainties. However, some solid points can be stated.

1) A steady uplift rate is not appropriate for fitting the constraints of the sea level markers. In UP1, uplift is mostly acquired between GIG 8 b and GIG 3a, with lower uplift rates in the other periods. Conversely, in UP2, much of the uplift is acquired between GIG 6 b and GIG 7 b, with only about 1.8 m of uplift afterwards. On the other hand, this observation is part of the concept of uplift rate sensitivity, exposed in Section 5.1. We would thus have periods of relative stasis of uplift that would be in agreement with some observations. For example, at

the base of the CL2 notches, the extensive abrasion platforms (Fig. 3B) could represent a stable RSL for an extended period of time. Periods of stasis should not be surprising, as they are also detectable along the Tyrrhenian side of Calabria. At Briatico, the fish-tank represented by the sea-level marker BRI (1 in Fig. 1) was constructed with a precise relationship to the sea level at ≈ 1645 cal Yr BP. Today, the Briatico fish-tank is still in connection with the sea-level (Anzidei et al., 2013). As there has been little to no non-tectonic sea level change since 1645 cal Yr BP, it follows that there has been little or no uplift since that time. But in this area, both the long-term uplift rate, calculated from the MIS 5.5 marine terrace elevation (Anzidei et al., 2013 and references therein) and the late Holocene uplift rates (Table 3) are at least 0.6 mm/yr. That is, Capo Vaticano seems to show a situation quite similar to the Crotona Peninsula, with long-term uplift rates greater than those on the short term.

2) The abandonment of coastline CL2 appears to have occurred abruptly, i.e., much faster than the rate of migration of the notch, thereby preserving the notch. Two sessile organisms (thus insensitive to resedimentation effects) dating the CL2 notch from two different localities, Spiaggia dei Gigli (GIG 3 b) and Curmo Beach (CUR 3), return the same age of 2300 cal Yr BP. This coincidence suggests that both chemical systems closed at the same time, corresponding to a rapid RSL drop. Although these are only two samples, it must be considered that sample SPR 0 could also be compatible with CL2. A similar sea-level marker from Spiagge Rosse was previously dated by Pirazzoli et al. (1997) at 2990 ± 60 yr B.P., with neither $\delta^{13}\text{C}$ nor reservoir corrections. SPR 0 is a calcareous, sessile seaweed with a ^{14}C age ranging between 2858 and 2345 cal Yr BP, thus partly overlapping with the age ranges of CUR 3 and GIG 3 b. Importantly, we didn't find any remains of intermediate coastlines between CL2 and the currently active coastline. The record of our coastlines forms a cluster at the age of CL2 around 2615 cal Yr BP, breaks around 2300 cal Yr BP and resumes only with the modern coastline markers.

One of the main problems in reconstructing the uplift path of an area concerns how to connect the constraints obtained from different sea-level markers. We could connect the different constraints with a

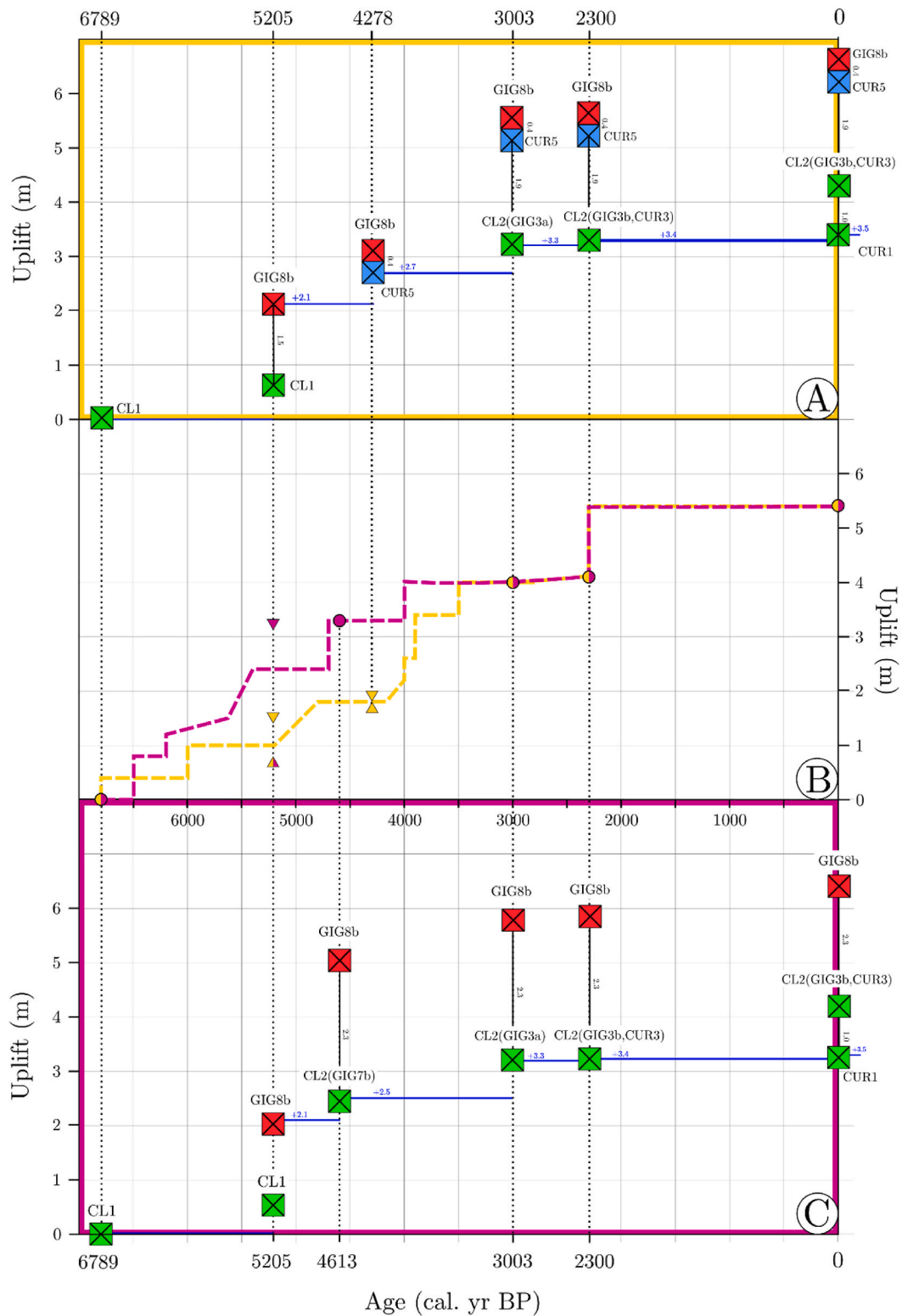


Fig. 11. | Uplift paths according to the two main hypothesis discussed in Section 5.2. Zero uplift occurs at 6789 cal Yr BP. RSL increase for GIA is marked by blue lines and blue numbers. A) Path1 (UP1) – the information from CUR 5 is valid. Squares are the sea level markers, colour depends on the original position with respect to the sea-level (blue under, green at, red above). B) Both paths are traced together: triangles are for upper and lower limits; circle is for a precise constraint of the sea-level. Yellow is for Path1, purple is for Path2. C) Path2 (UP2) – the information from GIG 7 b is valid. Squares are the sea level markers, colour depends on the original position with respect to the sea-level (blue under, green at, red above).

straight line to indicate that the area was affected by a steady uplift. A different option is to assume that the total uplift of an area was achieved with a series of coseismic pulses, as might have been the case for the CL2 coastline. However, we cannot rule out periods of accelerated uplift rate, i.e., a hybrid solution between the two previous options. Unfortunately, the ecological characteristics of the Mediterranean do not provide such high resolution RSL tracers. Discontinuous, or even reverse, vertical velocities appear to be typical of various subduction arcs. For example, U–Th dating on corals in the Sumatra Arc allows for high temporal resolution of RSL variations. The paleo-sea level record reveals a strongly discontinuous uplift process, consisting of rapid coseismic uplift events and interseismic periods of weak subsidence (Sieh et al., 2008). However, the summation of vertical contributions over the long term leads to a general uplift of the sector. In any case, coseismic uplift events along the coasts of subduction arcs are common. For example, along the Chilean subduction zone, a co-seismic uplift of 1.8 m with a Mw 8.1 earthquake was recorded (Ortlieb et al., 1996). Coseismic uplift of at least 1 m affected the coastline of the Peninsula de Nicoya, within the northern Costa Rican forearc, during the M 7.7 Nicoya subduction earthquake of October 5, 1950 (Martinez et al., 2018). Subsequently, in the postseismic period, four decades of gradual subsidence reversed a significant portion of this uplift (Martinez et al., 2018). In the Mediterranean subduction zones, earthquakes on reverse faults also produced

0.7 m of coseismic uplift in Algeria (Mw 6.8, Meghraoui et al., 2004), whereas in the Eastern Mediterranean (Crete subduction zone), the coseismic uplift due to the Mw 8.3 earthquake of 365 C E (Shaw et al., 2008) was as much as 9 m! Uplift of fossil coastlines along the Tyrrhenian side of Calabria has been interpreted as due to a series of coseismic pulses as well (Ferranti et al., 2017), driven by elastic rebound along the hanging walls of a series of coastal normal faults. In the case of Ionian Calabria, a co-seismic uplift mechanism would explain not only the short- and long-term difference in the uplift rates, but also the evidence for rapid abandonment of the CL2 coastline. It is less understood which source, if any, is capable for giving a such large displacement at the surface.

The DISS seismogenic source database (DISS 3.3.0 - DISS Working Group (2021)) reports a reverse fault as potential active seismogenic source, offshore the Crotone Peninsula (Fig. 12A). This structure is called the Crotone-Rossano Fault (CRF), and is a complex source formed by three segments with a slightly differing strikes (Fig. 12A). Following the characteristics of the CRF and assuming different magnitudes, we modelled the vertical displacement field in the case of activation of such a structure. We used the Okada (1985) model for finite deformation from a rectangular source in a homogeneous elastic half-space (see methods, Section 3.4). The maximum possible magnitude, as reported by the catalogue (Basili et al., 2008), is Mw 7.3. This earthquake would

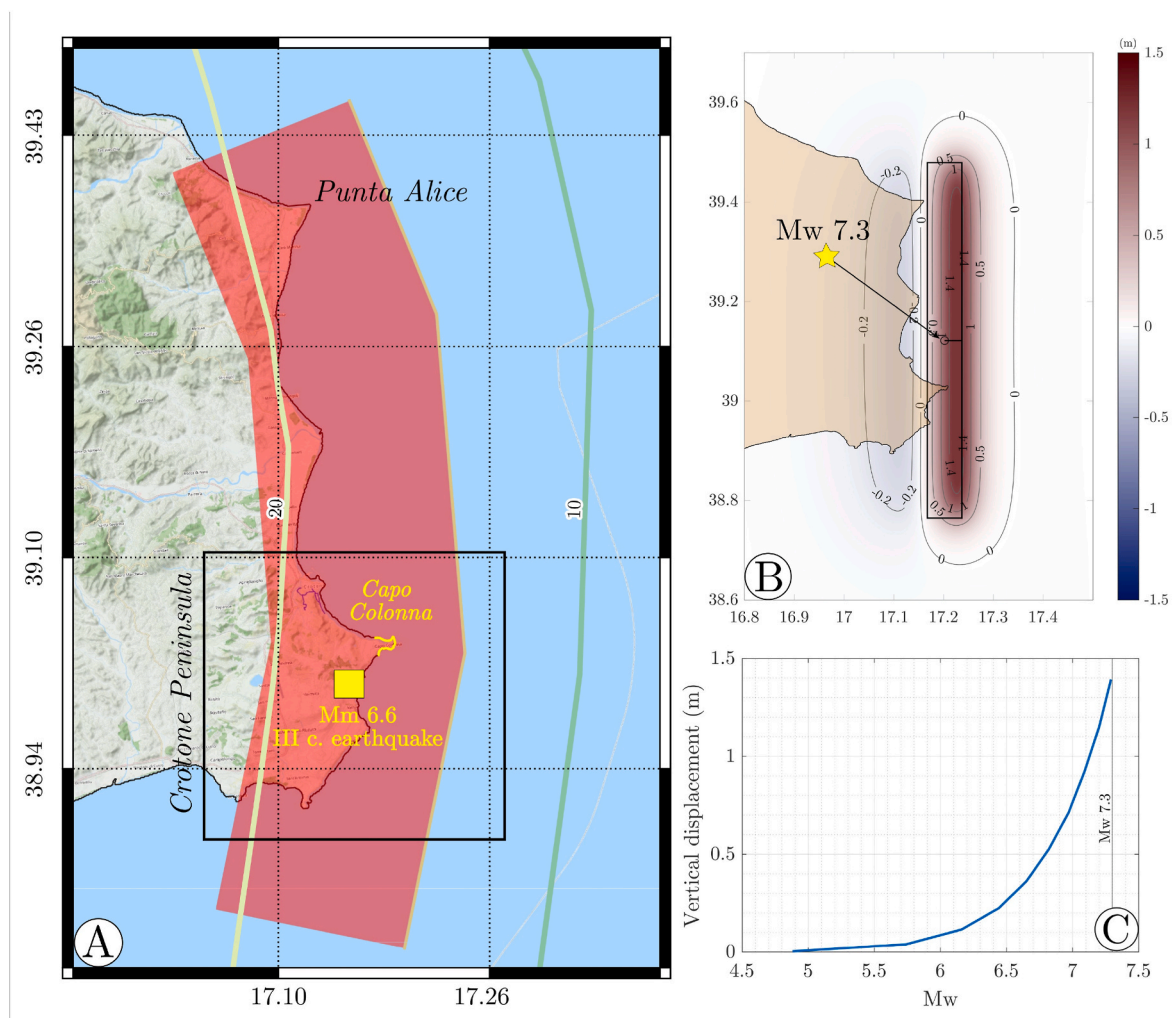


Fig. 12. | Model of the seismogenic source responsible for the postulated coseismic uplift of shoreline CL2. A) Surface projection of the Crotone-Rossano Fault (CRF, red area). The isobaths of the slab at 10 and 20 km, and the location of the third century CE earthquake are shown (Galli et al., 2006). B) Vertical displacement resulting from the activation of the whole fault plane with a Mw 7.3 seismic event. C) Variation of maximum uplift with seismic event of different magnitude. Each magnitude corresponds to a different rupture patch; the geometries are shown in Tab.4.

occur in case of a total rupture of the CRF, which shows dimensions of 80×9 km.

In our model, the geometry of the fault has been simplified to a single rectangle of the above dimensions. For this reason, it must be considered that the deformation obtained in our model is geographically shifted from that which would be obtained in the real case of activation. Thus, our results are useful only for a qualitative evaluation of the deformation pattern at the surface. To have a more precise geographic location of the vertical deformation, the real geometry of the seismogenic source should be included in the model.

Our model shows that an earthquake of Mw 7.3 sourced by a rectangular fault placed offshore the Crotona Peninsula can generate a maximum of 1.4 m of uplift (Fig. 12B). If we considered the true complex geometry of CRF, this maximum displacement would probably be centered exactly on the coast of the Crotona Peninsula. Furthermore, it can be seen in Fig. 12C and Table 4 that it is not necessary to activate the entire fault to have significant vertical deformation. Even with a Mw 7.0 to 7.1 earthquake, which would rupture between 47% and 63% of the entire CRF fault, there would be an uplift of 0.71–0.92 m (Table 4). Moreover, over longer time periods, the vertical deformation resulting from multiple high-magnitude earthquakes would be summed in the intersecting sectors. An earthquake of Mw 6.5, for example, would originate from a rupture of $\approx 20\%$ of the CRF fault plane and would produce ≈ 30 cm of vertical displacement at the surface. However, two or three earthquakes of this magnitude, rupturing patches at different depths, could generate a larger uplift signal at the surface. Thus, a cluster of earthquakes of different magnitudes may also represent a source of uplift. If they occurred over a short time-span, the uplift may not be properly coseismic, but it can be considered quasi-impulsive.

If a seismic event of Mw > 7 or a series of smaller events are capable of uplifting the Crotona Peninsula, it remains to be investigated whether or not earthquakes with these characteristics are present in the historical

Table 4

| Variation of fault parameters and surface vertical displacement depending on magnitude. 1) Moment magnitude was calculated using $M_w = 2/3 \log(M_0) - 6.07$ (Hanks and Kanamori, 1979); 2) Vertical displacement is the surface deformation value obtained with our model; 3) Fault slip is scaled to the fault size according to Wells and Coppersmith (1994) (see methods, Section 3.4); 4) Fault length is the largest side of the rectangular rupture; 5) Fault Width is the smallest side of the fault, equal to 11.25% of Fault Length. DISS geometry of the CRF is 80×9 km (100:11.25); 6) Rupture Area (Length x Width); 7) Percentage of rupture over the maximum area of the fault (corresponding to earthquake Mw max 7.3). The parameters of the maximum allowable rupture are shown in bold. Fixed parameters (Strike, Dip Angle and Rake) are reported in the last line.

Mw ¹	Vertical Displacement ² (m)	Fault Slip ³ (m)	Fault Length ⁴ (m)	Fault Width ⁵ (m)	Total surface ⁶ (m ²)	% of rupture ⁷
4.9	0	0.3	5000	563	2.81 E+06	0
5.7	0.04	0.8	13,333	1500	2.00 E+07	3
6.2	0.12	1.3	21,667	2438	5.28 E+07	7
6.4	0.22	1.8	30,000	3375	1.01 E+08	14
6.7	0.36	2.3	38,333	4313	1.65 E+08	23
6.8	0.53	2.8	46,667	5250	2.45 E+08	34
7	0.71	3.3	55,000	6188	3.40 E+08	47
7.1	0.92	3.8	63,333	7125	4.51 E+08	63
7.2	1.15	4.3	71,667	8063	5.78 E+08	80
7.3	1.39	4.8	80,000	9000	7.20 E+08	100

Strike = N180°, Dip Angle = 30°, Rake = 90°.

record of the Crotona Peninsula. The Crotona Peninsula has been inhabited for thousands of years, as evidenced by a great number of archaeological sites (i.e., Capo Colonna, Capo Piccolo, Le Castella). Therefore, it can be assumed that an earthquake of this magnitude left traces both in ancient and modern settlements. Many earthquakes have been historically detected in the area, but only one, which occurred in the 3rd century CE (macroseismic Magnitude Mm 6.6; Galli et al., 2006), had an epicenter compatible with the activation of a CRF patch (Fig. 12A). Unfortunately, this earthquake does not have a well-constrained source (Galli et al., 2006). According to the authors, the earthquake was responsible for the ultimate collapse and abandonment of the Roman settlement of Capo Colonna (Fig. 12A). The collapse of this settlement has been dated to the first half of the 3rd century CE, as indicated by the age of the coins and pottery sherds found below the collapsed roofs. Given its epicentral location, this earthquake would be a strong candidate for the source of the coseismic uplift of CL2 shoreline, but its age is too young. According to the CUR 3 and GIG 3 b sea-level markers, the youngest limit for the abandonment of CL2 shoreline is around the second half of the 1st BCE, while the earthquake occurred at least 250–300 yr later. The earthquake may, however, have contributed to bringing CL2 sea-level markers to their present elevations. Galli et al. (2006) suggested that there may have been other seismic events before this one in the area. Indeed, one of the domus in the Roman settlement at Capo Colonna was restored and then abandoned for no obvious reason in the first half of the 1st century CE. Given these archaeological observations, a cluster of discrete uplift events might be favoured over a single seismic event to explain the Holocene uplift of the Crotona Peninsula.

Given the many uncertainties surrounding the coseismic uplift of the CL2 sea-level markers, it is not possible to determine whether or not it was actually affected by an impulsive uplift. The CRF is indeed a seismogenic source capable of producing this deformation, but, as stated before, there is no correspondence between the chronological constraints of the uplift (1st century BCE, second half) and those of the Capo Colonna earthquake (3rd century CE, first half). However, further investigation on the uplift mechanism of this area should be addressed, since the confirmation of an active seismogenic source could significantly contribute to improve our understanding of the seismic and tsunami hazard of the Ionian coastal area of Calabria.

6. Conclusions

15 new AMS ¹⁴C dates allow us to constrain details of the Holocene uplift history of the Ionian coastal area of Calabria, particularly for the Crotona Peninsula. Unlike the Tyrrhenian side of Calabria, the Ionian coastal area has long remained under-studied. Only one sea-level marker indicating Holocene uplift was dated by Pirazzoli et al. (1997). Despite uncertainties due to the limited temporal resolution of the methodology used, as well as the discontinuous dataset, our new data on the Holocene sea-level markers of the Crotona Peninsula allow to draw the following conclusions.

- 1) The Ionian coast of Calabria, as well as the Tyrrhenian side of the region, experienced uplift in the late Holocene. The total uplift of about 5–6 m was achieved in the last ≈ 7 kyr.
- 2) The late Holocene uplift rate has not been steady. Time constraints from the available sea level markers define variable uplift rates through time.
- 3) The uplift rate calculated for the oldest Holocene shoreline, at about 7 ka, agrees with the middle-to-late Pleistocene uplift rate of 0.8 mm/yr. In contrast, for the younger Holocene shoreline, we find an uplift rate of only 0.5–0.6 mm/yr. However, this difference in uplift rate may be only apparent. If, in the near future this area would acquire a new discrete pulse of uplift, calculated Holocene and Pleistocene uplift rates would show little difference. We have summarized this reasoning with a concept called uplift rate sensitivity (Section 5.1).

Despite these insights, some questions related to the Holocene uplift history of the Crotona Peninsula remain unanswered. For example, the Holocene uplift path is not completely understood, and the specific causes of uplift are not yet identifiable. Some evidence suggest that the most recent fossil shoreline gained its current elevation with a rapid pulse of uplift. If confirmed, we need to identify a mechanism capable of producing surface deformation and uplift in a very short or even impulsive event.

Our tectonic model reveals that the CRF is a seismogenic source capable for producing up to 1.4 m of coseismic uplift with a Mw 7.3 earthquake. Whether or not it is responsible for CL2 shoreline uplift is unclear. A 3rd century CE earthquake may have contributed to raising the CL2 shoreline to its current elevation, even though it occurred 250–300 years later than the abandonment age of the shoreline. Another option is that a cluster mechanism of >Mw 6.5 earthquakes can account for the shoreline uplift, but evaluating this hypothesis will require more evidence.

Future research is needed to further investigate the uplift mechanism that affected the Ionian side of the Calabrian Arc in the late Holocene, considering that any seismogenic source could still be active. If it is the case, the seismic and tsunami hazard in the area should be updated and more deeply investigated. In addition, given the current rate of sea level rise, if the uplift path of the Crotona Peninsula has shown long periods of uplift rate close to zero, the flooding hazard in the area would need to be assessed.

A first step in resolving the open questions arose from this work is the integration of paleo-shoreline studies with geodetic measurements of the current vertical velocity field of the Crotona Peninsula.

Sitography

DISS 3.3.0 - DISS Working Group (2021). Database of Individual Seismogenic Sources (DISS), Version 3.3.0: A compilation of potential sources for earthquakes larger than M 5.5 in Italy and surrounding areas. Istituto Nazionale di Geofisica e Vulcanologia (INGV). <https://doi.org/10.13127/diss3.3.0>.

Beauducel F. (2022). Okada: Surface deformation due to a finite rectangular source (<https://www.mathworks.com/matlabcentral/fileexchange/25982-okada-surface-deformation-due-to-a-finite-rectangular-source>), MATLAB Central File Exchange.

ISPRA CARG project 577-Isola di Capo Rizzuto and 571-Crotona (https://www.isprambiente.gov.it/Media/carg/571_CROTONA/Foglio.html)

ISPRA CARG project 561-San Giovanni in Fiore https://www.isprambiente.gov.it/Media/carg/561_SGIOVANNI_FIORE/Foglio.html.

Fare clic o toccare se si considera attendibile questo collegamento.">https://www.isprambiente.gov.it/Media/carg/561_SGIOVANNI_FIORE/Foglio.html.

Author contribution

All authors participated in planning and supervising the research. M. L. and D.C. carried out the fieldwork, E.G. provided palaeontological advice, and P.C. assisted in the interpretation of the results. M.L. drafted the original manuscript, while D.C., E.G., and P.C. carried out internal reviews and contributed to the final version.

Declaration of competing interest

The authors declare that they have no known competing financial interests or personal relationships that could have appeared to influence the work reported in this paper.

Data availability

Data are shared through Mendley link. Codes for models are

opensource.

Acknowledgments

The grant to the Department of Science of Roma Tre University (MIUR—Italy Department of Excellence, article 1, paragraph 314–337, law 232/2016) is gratefully acknowledged. We would like to thank Daniele Melini and Giorgio Spada, for calculating the sea level curves and for providing support in the analysis. Thanks also to Taylor Schildgen for valuable scientific advice and English language review.

Appendix A. Supplementary data

Supplementary data to this article can be found online at <https://doi.org/10.1016/j.quascirev.2023.108368>.

References

- Antonoli, F., Silenzi, S., Vittori, E., Villani, C., 1999. Sea level changes and tectonic mobility: precise measurements in three coastlines of Italy considered stable during the last 125 kyr. *Phys. Chem. Earth Solid Earth Geodes.* 24 (4), 337–342.
- Antonoli, F., Ferranti, L., Lambeck, K., Kershaw, S., Verrubbi, V., Dai Pra, G., 2006. Late Pleistocene to Holocene record of changing uplift rates in southern Calabria and northeastern Sicily (southern Italy, central Mediterranean sea). *Tectonophysics* 422 (1–4), 23–40.
- Antonoli, F., Presti, V.L., Rovere, A., Ferranti, L., Anzidei, M., Furlani, S., et al., 2015. Tidal notches in Mediterranean Sea: a comprehensive analysis. *Quat. Sci. Rev.* 119, 66–84.
- Anzidei, M., Antonoli, F., Benini, A., Gervasi, A., Guerra, I., 2013. Evidence of vertical tectonic uplift at Briatico (Calabria, Italy) inferred from Roman age maritime archaeological indicators. *Quat. Int.* 288, 158–167.
- Barrier, P., 1990. Faune Senegalienne du paleoscarpement du Capo Vaticano (Calabre meridionale), Implications neotectoniques. In: *Atti del Quarto Simposio di Ecologia e Paleocologia delle Comunità Bentoniche*, pp. 511–526. Sorrento.
- Basili, Roberto, et al., 2008. The Database of Individual Seismogenic Sources (DISS), version 3: summarizing 20 years of research on Italy's earthquake geology. *Tectonophysics* 453 1–4, 20–43.
- Bianca, M., Catalano, S., De Guidi, G., Gueli, A.M., Monaco, C., Ristuccia, G.M., et al., 2011. Luminescence chronology of Pleistocene marine terraces of Capo Vaticano peninsula (Calabria, southern Italy). *Quat. Int.* 232 (1–2), 114–121.
- Bordoni, P., Valensise, G., 1999. Deformation of the 125 ka marine terrace in Italy: tectonic implications. Geological Society, London, Special Publications 146 (1), 71–110.
- Braitenberg, C., Mariani, P., Tunini, L., Grillo, B., Nagy, I., 2011. Vertical crustal motions from differential tide gauge observations and satellite altimetry in southern Italy. *J. Geodyn.* 51 (4), 233–244.
- Capozzi, R., Artoni, A., Torelli, L., Lorenzini, S., Oppo, D., Mussoni, P., Polonia, A., 2012. Neogene to quaternary tectonics and mud diapirism in the gulf of Squillace (Crotona-Spartivento basin, Calabrian Arc, Italy). *Mar. Petrol. Geol.* 35 (1), 219–234.
- Carobene, L., Dai-Pra, G., Gewalt, M., 1986. Niveaux marins du Pléistocène moyen-supérieur de la côte tyrrhénienne de la Calabre (Italie méridionale) Datations ²³⁰Th/²³⁴U et tectonique récente. *Z. Geomorphol. - Suppl.* 62, 141–158.
- Cerrone, C., Vacchi, M., Fontana, A., Rovere, A., 2021. Last interglacial sea-level proxies in the western Mediterranean. *Earth Syst. Sci. Data* 13 (9), 4485–4527.
- Cosentino, D., Gliozzi, E., 1988. Considerazioni sulle velocità di sollevamento di depositi eutirreniani dell'Italia meridionale e della Sicilia. *Memor. Soc. Geol. Ital.* 41, 653–665.
- Cosentino, D., Gliozzi, E., Salvini, F., 1989. Brittle deformations in the upper Pleistocene deposits of the Crotona peninsula, Calabria, southern Italy. *Tectonophysics* 163 (3–4), 205–217.
- Cucci, L., 2004. Raised marine terraces in the Northern Calabrian Arc (Southern Italy): a 600 kyr-long geological record of regional uplift. *Ann. Geophys.* 47 (4), 1391–1406.
- Dai Pra, G., Miyauchi, T., Anselmi, B., Galletti, M., Paganin, G., 1992. Età dei depositi a Strombus bubonius di Vibo Valentia Marina (Italia meridionale). *Il Quat.* 6 (1), 139–144.
- Dumas, B., Guérémy, P., Lhénaff, R., Raffy, J., 1995. Reconstitution morphométrique d'un dispositif de paléorivages soulevés dans un relief de dissection en Locride (Calabre Ionienne, Italie). *Geodin. Acta* 8 (4), 185–198.
- Dumas, B., Raffy, J., 1996. Enregistrement géomorphologique de maxima glacio-eustatiques dans la région soulevée de Soverato (Italie du sud). *Bull. Soc. Geol. Fr.* 167 (2), 285–293.
- Faccenna, C., Jolivet, L., Piromallo, C., Morelli, A., 2003. Subduction and the depth of convection in the Mediterranean mantle. *J. Geophys. Res. Solid Earth* 108 (B2).
- Ferranti, L., Antonoli, F., Mauz, B., Amorosi, A., Dai Pra, G., Mastronuzzi, G., et al., 2006. Markers of the last interglacial sea-level high stand along the coast of Italy: tectonic implications. *Quat. Int.* 145, 30–54.
- Ferranti, L., Monaco, C., Antonoli, F., Maschio, L., Kershaw, S., Verrubbi, V., 2007. The contribution of regional uplift and coseismic slip to the vertical crustal motion in the Messina Straits, Southern Italy: evidence from raised Late Holocene shorelines. *J. Geophys. Res. Solid Earth* 112 (B6).

- Ferranti, L., Antonioli, F., Scicchitano, G., Spampinato, C.R., 2017. Uplifted Late Holocene shorelines along the coasts of the Calabrian Arc: geodynamic and seismotectonic implications. *Italian J. Geosci.* 136 (3), 454–470.
- Galli, P., Ruga, A., Scionti, V., Spadea, R., 2006. Archaeoseismic evidence for a late roman earthquake in the Crotona area (Ionian Calabria, southern Italy): seismotectonic implications. *J. Seismol.* 10 (4), 443–458.
- Gliozzi, E., 1988. I terrazzi marini del Pleistocene superiore della penisola di Crotona (Doctoral dissertation, Ph. D. thesis, Università degli Studi di Napoli, Naples, Italy).
- Hanks, T.C., Kanamori, H., 1979. A moment magnitude scale. *J. Geophys. Res. Solid Earth* 84 (B5), 2348–2350.
- Laborel, J., Laborel-Deguen, F., 1996. Biological indicators of Holocene sea-level and climatic variations on rocky coasts of tropical and subtropical regions. *Quat. Int.* 31, 53–60.
- Lambeck, K., Antonioli, F., Purcell, A., Silenzi, S., 2004. Sea-level change along the Italian coast for the past 10,000 yr. *Quat. Sci. Rev.* 23 (14–15), 1567–1598.
- Lambeck, K., Antonioli, F., Anzidei, M., Ferranti, L., Leoni, G., Scicchitano, G., Silenzi, S., 2011. Sea level change along the Italian coast during the Holocene and projections for the future. *Quat. Int.* 232 (1–2), 250–257.
- Liberatore, M., Gliozzi, E., Cipollari, P., Ögretmen, N., Spada, G., Cosentino, D., 2022. Vertical velocity fields along the Eastern Mediterranean coast as revealed by late Holocene sea-level markers. *Earth Sci. Rev.* 234.
- Lougheed, B., Obrochta, S., 2016. MatCal: open source bayesian 14 C age calibration in MatLab. *J. Open Res. Software* 4 (1).
- Magri, G., Sidoti, G., Spada, A., 1963. Rilevamento Geologico Sul Versante Settentrionale Della Sila. Calabria.
- Martinez, Z., Klemann, V., van der Wal, W., Riva, R.E.M., Spada, G., Sun, Y., et al., 2018. A benchmark study of numerical implementations of the sea level equation in GIA modelling. *Geophys. J. Int.* 215 (1), 389–414.
- Massari, F., Prosser, G., 2013. Late Cenozoic tectono-stratigraphic sequences of the Crotona Basin: insights on the geodynamic history of the Calabrian arc and Tyrrhenian Sea. *Basin Res.* 25 (1), 26–51.
- Mauz, B., Hassler, U., 2000. Luminescence chronology of Late Pleistocene raised beaches in southern Italy: new data of relative sea-level changes. *Mar. Geol.* 170 (1–2), 187–203.
- Mauz, B., Vacchi, M., Green, A., Hoffmann, G., Cooper, A., 2015. Beachrock: a tool for reconstructing relative sea level in the far-field. *Mar. Geol.* 362, 1–16.
- Meghraoui, M., Maouche, S., Chema, B., Cakir, Z., Aoudia, A., Harbi, A., et al., 2004. Coastal uplift and thrust faulting associated with the Mw= 6.8 Zemmouri (Algeria) earthquake of 21 May, 2003. *Geophys. Res. Lett.* 31 (19).
- Miyauchi, T., 1994. Geochronology of Pleistocene marine terraces and regional tectonics in the Tyrrhenian coast of South Calabria. *Il Quat.* 7, 17–34.
- Monaco, C., Barreca, G., Di Stefano, A., 2017. Quaternary marine terraces and fault activity in the northern mainland sectors of the Messina Strait (southern Italy). *Italian Journal of Geosciences* 136 (3), 337–346.
- Nalin, R., Lamothe, M., Auclair, M., Massari, F., 2020. Chronology of the marine terraces of the Crotona Peninsula (Calabria, southern Italy) by means of infrared-stimulated luminescence (IRSL). *Mar. Petrol. Geol.* 122, 104645.
- Nalin, R., Bracchi, V.A., Basso, D., Massari, F., 2012. Persististrombus latus (Gmelin) in the upper Pleistocene deposits of the marine terraces of the Crotona peninsula (southern Italy). *Italian J. Geosci.* 131 (1), 95–101.
- Ogniben, L., 1973. Schema Geologico Della Calabria in Base Ai Dati Odierni.
- Okada, Y., 1985. Surface deformation due to shear and tensile faults in a half-space. *Bull. Seismol. Soc. Am.* 75 (4), 1135–1154.
- Ortlieb, L., Barrientos, S., Guzman, N., 1996. Coseismic coastal uplift and coralline algae record in northern Chile: the 1995 Antofagasta earthquake case. *Quat. Sci. Rev.* 15 (8–9), 949–960.
- Peltier, W.R., Argus, D.F., Drummond, R., 2015. Space geodesy constrains ice age terminal deglaciation: the global ICE-6G_C (VM5a) model. *J. Geophys. Res. Solid Earth* 120 (1), 450–487.
- Pirazzoli, P.A., Mastronuzzi, G., Saliege, J.F., Sansò, P., 1997. Late Holocene emergence in Calabria, Italy. *Mar. Geol.* 141 (1–4), 61–70.
- Roy, K., Peltier, W.R., 2018. Relative sea level in the Western Mediterranean basin: a regional test of the ICE-7G_NA (VM7) model and a constraint on late Holocene Antarctic deglaciation. *Quat. Sci. Rev.* 183, 76–87.
- Serpelloni, E., Faccenna, C., Spada, G., Dong, D., Williams, S.D., 2013. Vertical GPS ground motion rates in the Euro-Mediterranean region: new evidence of velocity gradients at different spatial scales along the Nubia-Eurasia plate boundary. *J. Geophys. Res. Solid Earth* 118 (11), 6003–6024.
- Sieh, K., Natawidjaja, D.H., Meltzner, A.J., Shen, C.C., Cheng, H., Li, K.S., et al., 2008. Earthquake supercycles inferred from sea-level changes recorded in the corals of west Sumatra. *Science* 322 (5908), 1674–1678.
- Shaw, B., Ambraseys, N.N., England, P.C., Floyd, M.A., Gorman, G.J., Higham, T.F.G., et al., 2008. Eastern Mediterranean tectonics and tsunami hazard inferred from the AD 365 earthquake. *Nat. Geosci.* 1 (4), 268–276.
- Spada, G., Melini, D., 2019. SELEN 4 (SELEN version 4.0): a Fortran program for solving the gravitationally and topographically self-consistent sea-level equation in glacial isostatic adjustment modeling. *Geosci. Model Dev. (GMD)* 12 (12), 5055–5075.
- Spampinato, C.R., Braitenberg, C., Monaco, C., Scicchitano, G., 2013. Analysis of vertical movements in eastern Sicily and southern Calabria (Italy) through geodetic leveling data. *J. Geodyn.* 66, 1–12.
- Spampinato, C.R., Ferranti, L., Monaco, C., Scicchitano, G., Antonioli, F., 2014. Raised Holocene paleo-shorelines along the Capo Vaticano coast (western Calabria, Italy): evidence of co-seismic and steady-state deformation. *J. Geodyn.* 82, 178–193.
- Tam, E., Yokoyama, Y., 2021. A review of MIS 5e sea-level proxies around Japan. *Earth Syst. Sci. Data* 13 (4), 1477–1497.
- Tortorici, G., Bianca, M., de Guidi, G., Monaco, C., Tortorici, L., 2003. Fault activity and marine terracing in the Capo Vaticano area (southern Calabria) during the middle-late quaternary. *Quat. Int.* 101, 269–278.
- Vacchi, M., Marriner, N., Morhange, C., Spada, G., Fontana, A., Rovere, A., 2016. Multiproxy assessment of Holocene relative sea-level changes in the western Mediterranean: sea-level variability and improvements in the definition of the isostatic signal. *Earth Sci. Rev.* 155, 172–197.
- Vousdoukas, M.L., Velegrakis, A.F., Plomaritis, T.A., 2007. Beachrock occurrence, characteristics, formation mechanisms and impacts. *Earth Sci. Rev.* 85 (1–2), 23–46.
- Wells, D.L., Coppersmith, K.J., 1994. New empirical relationships among magnitude, rupture length, rupture width, rupture area, and surface displacement. *Bull. Seismol. Soc. Am.* 84 (4), 974–1002.
- Zecchin, M., Nalin, R., Roda, C., 2004. Raised Pleistocene marine terraces of the Crotona peninsula (Calabria, southern Italy): facies analysis and organization of their deposits. *Sediment. Geol.* 172 (1–2), 165–185.
- Zecchin, M., Caffau, M., Civile, D., Critelli, S., Di Stefano, A., Maniscalco, R., et al., 2012. The Plio-Pleistocene evolution of the Crotona Basin (southern Italy): interplay between sedimentation, tectonics and eustasy in the frame of Calabrian Arc migration. *Earth Sci. Rev.* 115 (4), 273–303.
- Zecchin, M., Accaino, F., Ceramicola, S., Civile, D., Critelli, S., Da Lio, C., et al., 2018. The Crotona Megalandslide, southern Italy: architecture, timing and tectonic control. *Sci. Rep.* 8 (1), 1–11.

Supplementary Material

Other sections witnessing a higher RSL than the current one are presented here. The description of each section is provided in the main text in Sec. 4.1.

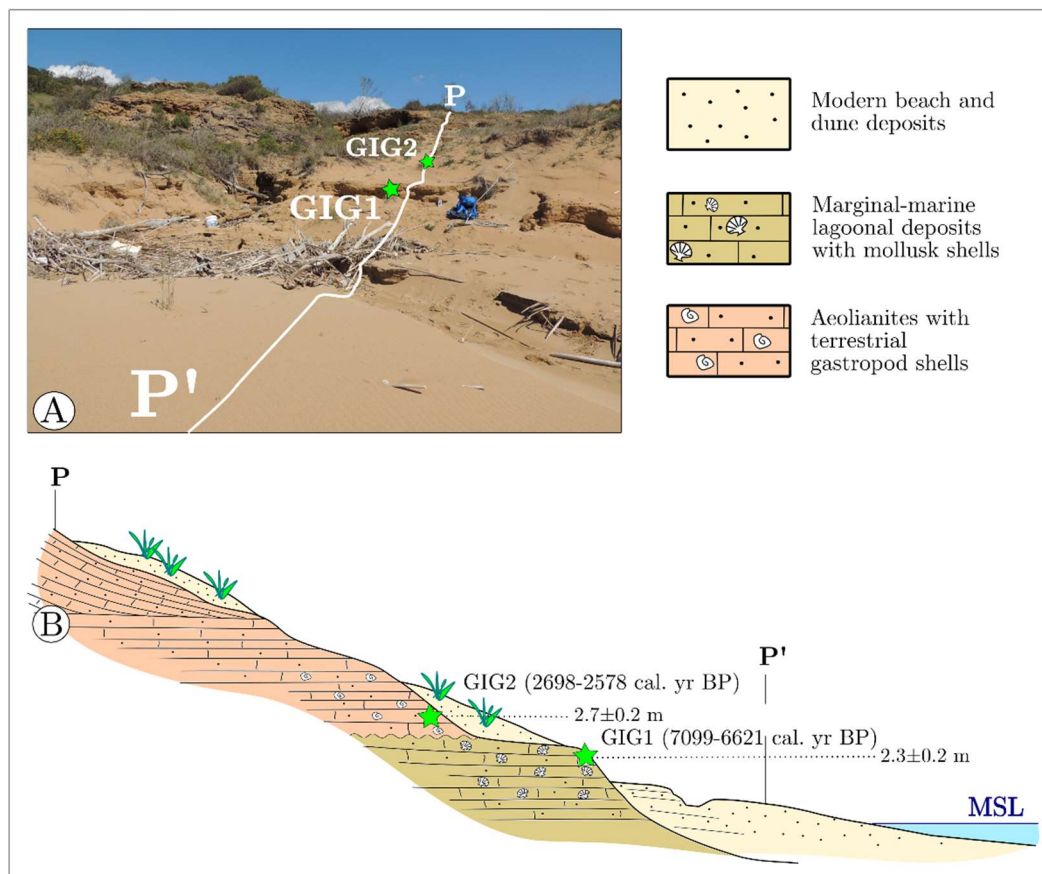


Figure S1 | Spiaggia dei Gigli: A) P-P' trace of Section 1; GIG 1 and GIG 2 samples are also shown; B) P-P' schematic geological section (See Fig. 3 for location)

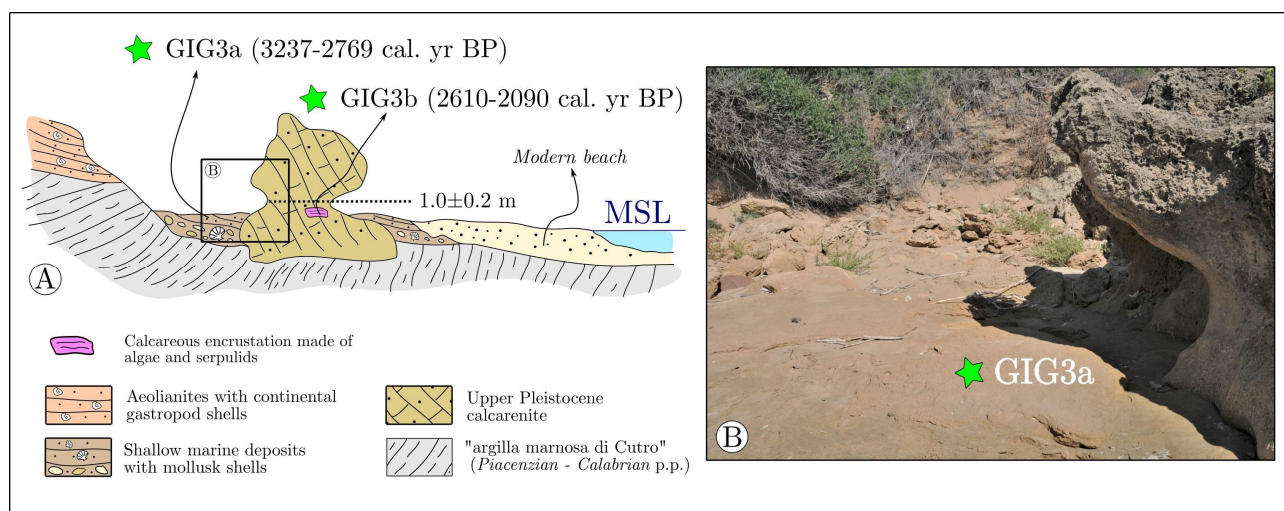


Figure S2 | Spiaggia dei Gigli, Section 2. A) Sketch of the mushroom-like notch at 1.0 ± 0.2 m a.m.s.l. B) picture of the notch at 1.0 ± 0.2 m a.m.s.l., the position of GIG 3a sample is also shown (See Fig.3).

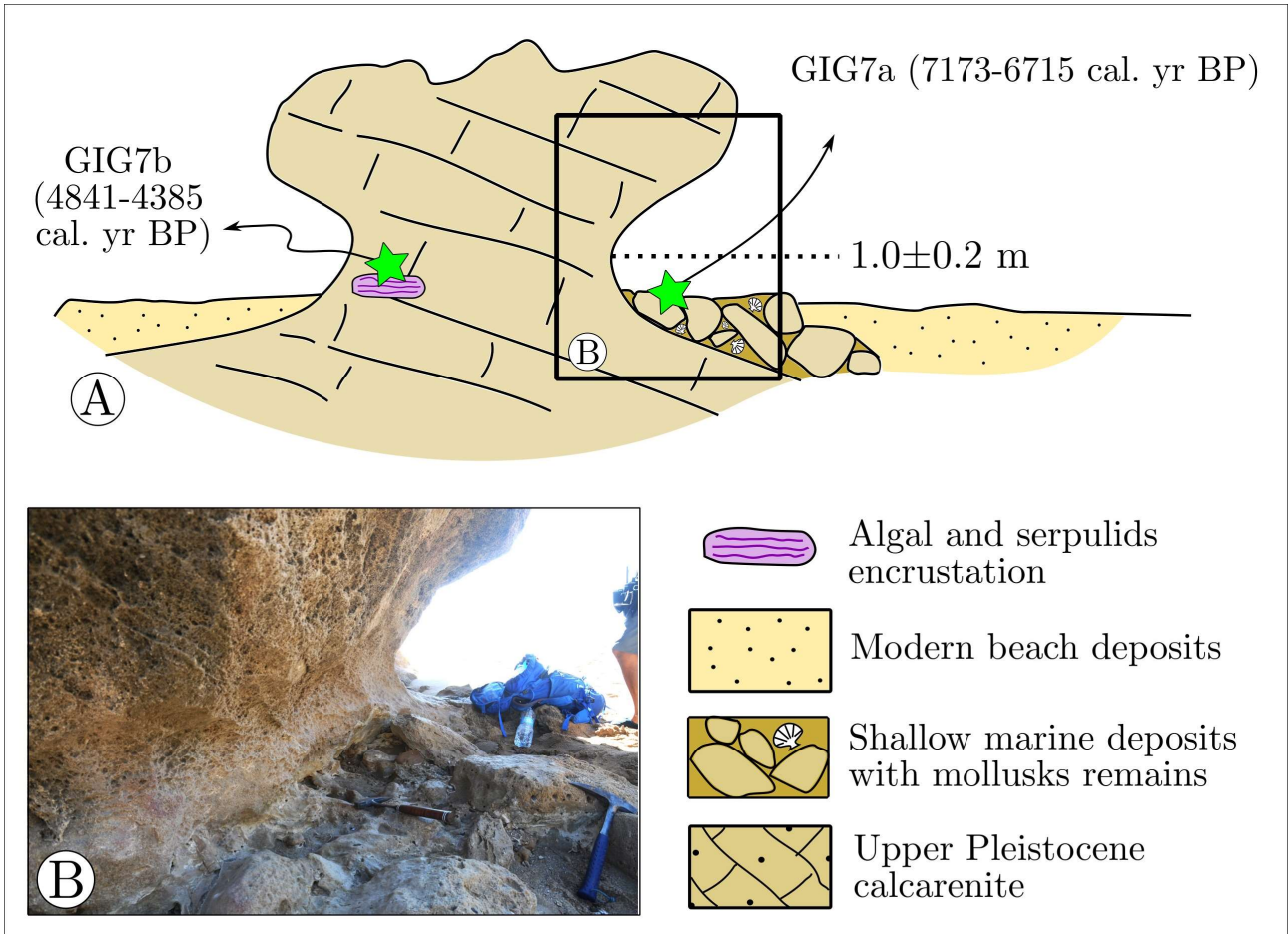


Figure S3 | Spiaggia dei Gigli, Section 3. A) sketch of the mushroom-shaped block showing the position of the collected samples for ^{14}C datings; B) picture of the 1.0 ± 0.10 m a.m.s.l. notch along Section 3. (See Fig.3 for location).

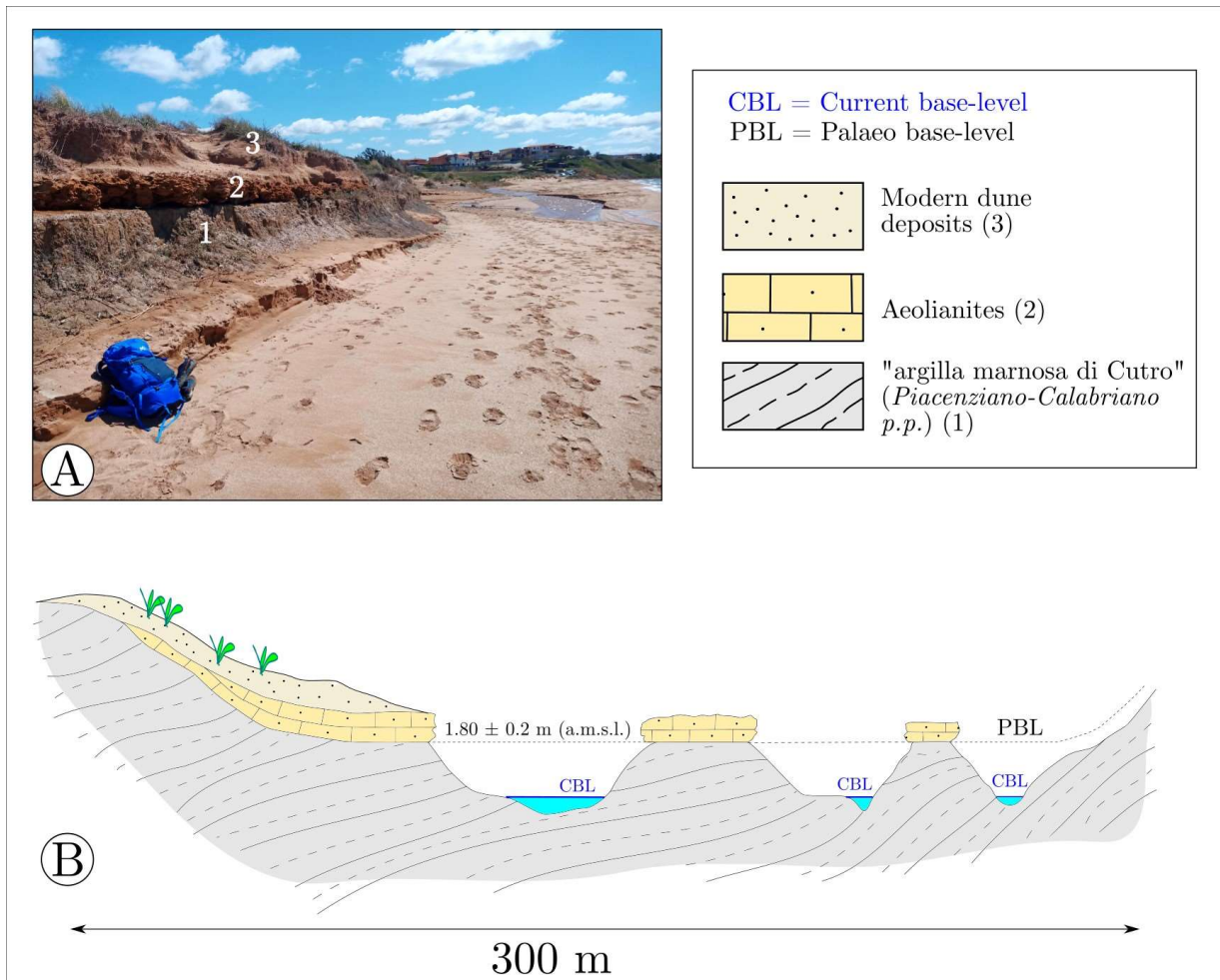


Figure S4 | Spiaggia di Selene. A) The picture shows a sharp horizontal unconformity between the "argilla marnosa di Cutro" (1) and the aeolianites (2). On top of the aeolianites current sand dunes are present (3). B) Sketch representing the flat unconformity between the "argilla marnosa di Cutro" and the aeolianites. Following the elevation of the unconformity, a paleo riverbed (corresponding to a paleo base-level) can be traced.

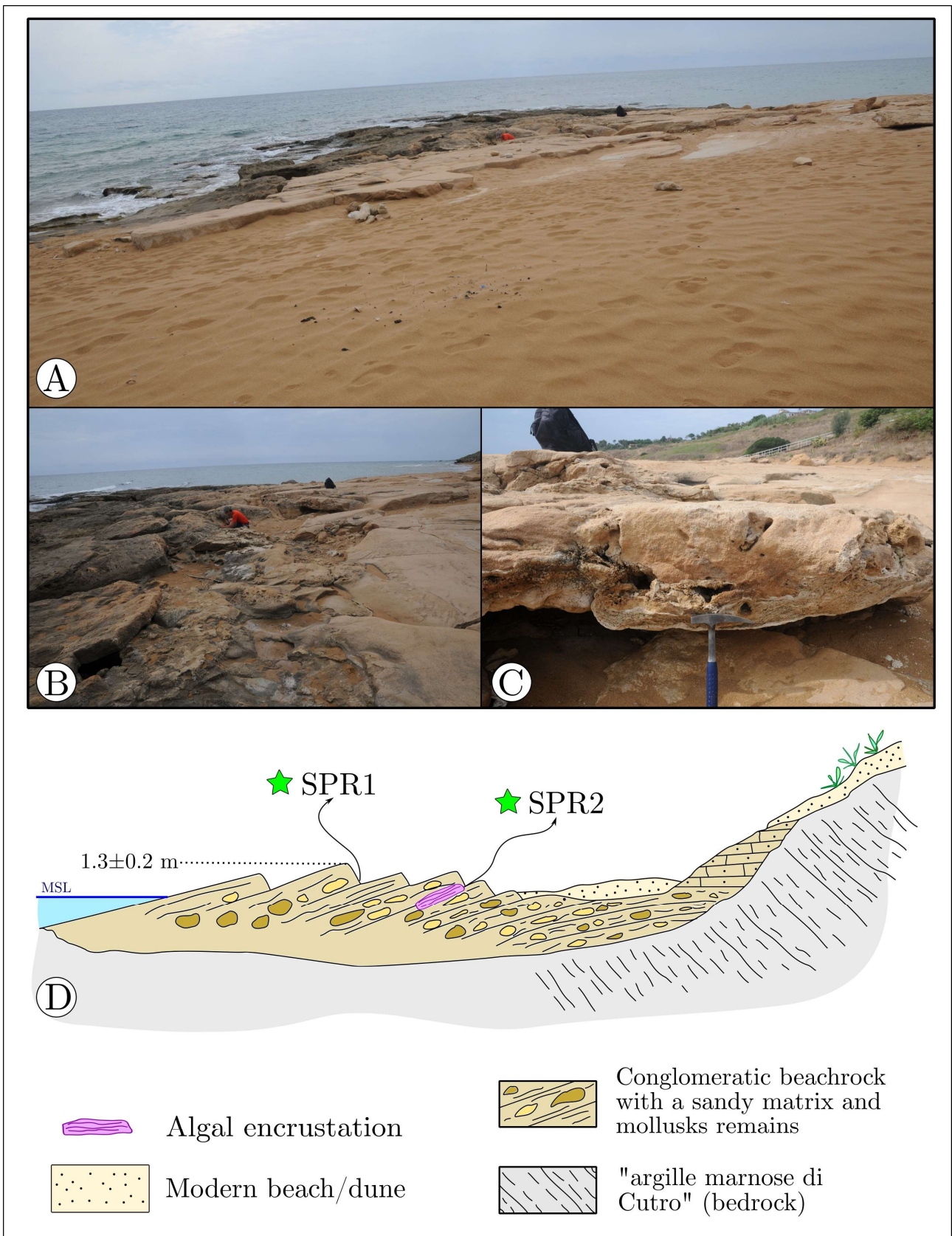


Figure S5 | Spiagge Rosse. A) Picture showing the beachrock cropping out at Spiagge Rosse, B) Different lithologies, consisting mainly of calcarenites and conglomerate, define the Spiagge Rosse beachrock, C) Detail of a calcareous encrustation made of serpulids and algae encrusting calcarenites of the beachrock (sample SPR2). D) Sketch of the beachrock showing its higher elevation and the position of the collected samples.



Figure S6 | Picture showing an active beachrock in Spiaggia di Curmo.